Recapitulation of Perturbed Striatal Gene Expression Dynamics of Donor's Brains With Ventral Forebrain Organoids Derived From the Same Individuals With Schizophrenia

Tomoyo Sawada, Ph.D., André R. Barbosa, Ph.D., Bruno Araujo, Ph.D., Alejandra E. McCord, B.A., Laura D'Ignazio, Ph.D., Kynon J.M. Benjamin, Ph.D., Bonna Sheehan, B.Sc., Michael Zabolocki, B.Sc., Arthur Feltrin, Ph.D., Ria Arora, B.Sc., Anna C. Brandtjen, B.A., Joel E. Kleinman, M.D., Ph.D., Thomas M. Hyde, M.D., Ph.D., Cedric Bardy, Ph.D., Daniel R. Weinberger, M.D., Apuã C.M. Paquola, Ph.D., Jennifer A. Erwin, Ph.D.

Objective: Schizophrenia is a brain disorder that originates during neurodevelopment and has complex genetic and environmental etiologies. Despite decades of clinical evidence of altered striatal function in affected patients, studies examining its cellular and molecular mechanisms in humans are limited. To explore neurodevelopmental alterations in the striatum associated with schizophrenia, the authors established a method for the differentiation of induced pluripotent stem cells (iPSCs) into ventral forebrain organoids (VFOs).

Methods: VFOs were generated from postmortem dural fibroblast−derived iPSCs of four individuals with schizophrenia and four neurotypical control individuals for whom postmortem caudate genotypes and transcriptomic data were profiled in the BrainSeq neurogenomics consortium. Individuals were selected such that the two groups had nonoverlapping schizophrenia polygenic risk scores (PRSs).

Results: Single-cell RNA sequencing analyses of VFOs revealed differences in developmental trajectory between schizophrenia and control individuals in which inhibitory neuronal cells from the patients exhibited accelerated maturation. Furthermore, upregulated genes in inhibitory neurons in schizophrenia VFOs showed a significant overlap with upregulated genes in postmortem caudate tissue of individuals with schizophrenia compared with control individuals, including the donors of the iPSC cohort.

Conclusions: The findings suggest that striatal neurons derived from high-PRS individuals with schizophrenia carry abnormalities that originated during early brain development and that the VFO model can recapitulate disease-relevant cell type−specific neurodevelopmental phenotypes in a dish.

AJP in Advance (doi: 10.1176/appi.ajp.20220723)

Schizophrenia affects approximately 1% of the world population and often causes lifelong chronic psychosocial disturbances (1). Both genetic and environmental factors drive the complex etiology of schizophrenia, which is expressed as a combination of psychotic symptoms and motivational and cognitive dysfunction (2). The biology of the disorder is poorly understood, at least in part because of heterogeneous phenotypes and the complex causal contributions of low-penetrant common alleles and highly penetrant but ultra-rare variants. A recent genome-wide association study (GWAS) revealed an enrichment of common variants in genes highly expressed in both excitatory and inhibitory neurons, including medium spiny neurons (MSNs) in the striatum. However, these variants were not specifically concentrated in any one brain region (3), suggesting that a brain-wide abnormal neuronal function underlies schizophrenia pathogenesis. Trubetskoy and colleagues also demonstrated the convergence of common and rare variant associations between schizophrenia and various neurodevelopmental disorders (3).

Neurodevelopmental abnormalities have long been proposed to play a pathogenic role in schizophrenia and are a cornerstone of the neurodevelopmental hypothesis of this illness (4). Schizophrenia risk is thought to start accumulating in utero and to be maintained and amplified throughout life (5). Given the disease's specificity to humans and the inaccessibility of pre-disease brain tissues, studying the molecular and cellular underpinnings of schizophrenia has been challenging. Human induced pluripotent stem cells (iPSCs) and recent progress in brain organoid technology

have enabled model building to simulate aspects of human brain development. Research with patient-derived iPSCs points to alterations in several neurodevelopmental pathways in schizophrenia, such as neural progenitor cell proliferation, imbalanced differentiation of excitatory and inhibitory cortical neurons, and altered Wnt signaling during neurogenesis (6). However, most studies have focused on neurodevelopmental dysfunction of cortical and/or excitatory neurons in the pathogenesis of the disorder.

Neuroimaging and neuropathological studies have demonstrated disordered connectivity between brain regions in schizophrenia (7–12). One of the brain regions with disrupted function and connectivity in schizophrenia is the striatum (13, 14). The striatum, made up principally of the caudate nucleus and putamen, is a central component of the basal ganglia that forms a complex neural circuit that is crucial for sensorimotor, cognitive, and emotional-motivational brain functions (15). Notably, most antipsychotics used to treat schizophrenia essentially rely on the blockade of D_2 dopamine receptors, which are most abundant in the striatum (16). Despite a potential central role in the pathogenesis of schizophrenia, the cellular and molecular underpinnings of striatal dysfunction related to the disorder have been understudied.

The MSNs, GABAergic projection neurons carrying either D_1 or D_2 dopamine receptors, are the principal striatal neuronal population (17, 18). MSNs receive excitatory glutamatergic inputs from the cerebral cortex and the thalamus and modulatory dopaminergic inputs from the midbrain (15). The remaining striatal neuronal population are aspiny interneurons, which comprise 23% of primate striatal neurons (19, 20) and are classified into cholinergic and GABAergic interneurons. GABAergic interneurons further fall into three main subtypes, expressing somatostatin (SST), parvalbumin (PV), or calretinin (21). During development, MSNs and interneurons originate from the subpallium, a part of the ventral forebrain. MSNs arise from progenitors in the lateral ganglionic eminence (LGE) (22–25), whereas the medial ganglionic eminence (MGE) gives rise to SST- and PV-expressing GABAergic interneurons in addition to cholinergic interneurons, and the caudal ganglionic eminence (CGE) produces calretinin-expressing GABAergic interneurons (24, 26, 27). In the present study, we sought to investigate neurodevelopmental alterations underlying the striatal pathogenesis of schizophrenia by simulating human striatal development in a dish with iPSC-derived ventral forebrain organoids (VFOs).

iPSC-based modeling has the potential to bring about a sea change in our understanding of the neurodevelopmental underpinnings of schizophrenia. However, there are important difficulties that still need to be addressed. First, schizophrenia is a polygenic disorder with a complex genetic architecture. Genes implicated in risk for the disorder show relatively greater expression during fetal than postnatal life (28, 29). Moreover, there is a significant overlap of GWAS risk loci between autism spectrum disorder (ASD) and schizophrenia (30). However, it is unclear how potential perturbations of early brain development translate into illness in adults. Second, validation of any brain organoid model of schizophrenia is problematic. This difficulty arises because there is no known morphological abnormality in fetal brains of individuals with schizophrenia, such as the increased brain size or macrocephaly observed in some individuals with ASD (31–33). Moreover, to our knowledge, the validity of iPSC-based schizophrenia models has not been well evaluated with postmortem brain analysis. Although it is assumed that both the monolayer neuronal culture and brain organoids derived from human iPSCs can recapitulate aspects of the late fetal stage of the developing brain, or preterm infancy at most (34), it remains to be established whether brain organoids can reproduce the disease-associated changes seen in the postmortem brain tissue of adults diagnosed with schizophrenia that possibly originate during the fetal stage.

Given the challenges of iPSC-based modeling of schizophrenia, in the present study we first tried to reduce heterogeneity of genetic risk by analyzing VFOs derived from four individuals with schizophrenia and from four neurotypical individuals; the individuals were selected such that the two groups had nonoverlapping polygenic risk scores (PRSs) for schizophrenia (35). We next assessed the validity of the VFO model of schizophrenia by comparing the findings from the organoids with the data from the postmortem caudate tissue of the iPSC donors and others.

METHODS

Tissue Collection

Postmortem dural tissue from four neurotypical Caucasian males (36) and four Caucasian males with schizophrenia were collected at autopsy (37–39), and fibroblasts were isolated from dura mater, as previously described (40). Participants were selected from the Lieber Institute for Brain Development (LIBD) brain repository (https://www.libd.org/brain-repository/) based on 1) the schizophrenia PRS (3, 41), 2) fibroblast availability, and 3) biological sex and self-identified race matching between groups. Collection and use for research of fibroblasts were approved by the Western Institutional Review Board. Dura-derived fibroblasts were grown and maintained as previously described (36).

PRSs are a measure of cumulative genomic risk (41), calculated as the sum of risk alleles of index single-nucleotide polymorphisms (SNPs) from GWASs, weighted for the strength of association (i.e., the odds ratio). Consistent with the standard procedure for PRS calculation (41), only autosomal SNPs were included in the analysis, and the major histocompatibility complex region was excluded because of its inherent complexity. As previously described (41–44), we performed linkage disequilibrium pruning and "clumping" of the SNPs, discarding variants within 500 kb of, and in $r^2 \geq 0.1$ with, another (more significant) marker. We

multiplied the natural log of the odds ratios of each index SNP by the imputation probability for the corresponding effective allele for the odds ratio at each variant, and we summed the products over all variants, so that each subject had whole-genome PRSs. Ten PRSs (PRS1–PRS10) were calculated using subsets of SNPs selected according to the GWAS p-value thresholds of association with schizophrenia: 5×10^{-8} (PRS1), 1×10^{-6} (PRS2), 1×10^{-4} (PRS3), 0.001 (PRS4), 0.01 (PRS5), 0.05 (PRS6), 0.1 (PRS7), 0.2 (PRS8), 0.5 (PRS9), and 1 (PRS10). PRS6 was employed to select the samples, following previous evidence (42) that it has the highest accuracy in predicting the respective disease or trait.

Generation and Maintenance of iPSCs
Dura-derived fibroblasts between passages 5 and 7 were reprogrammed with Sendai virus (SeV) with CytoTune-iPS 2.0 (Thermo Fisher Scientific) following the manufacturer's instructions or episomal vectors (45). Plasmids pCXLE-hOCT3/4-shp53-F (Addgene 27077), pCXLE-hSK (27078), and pCXLE-hUL (27080) were transfected into fibroblasts using a 4D-Nucleofector system with P2 Primary Cell 4D-Nucleofector X Kit (Lonza; program DT-130). Single iPSC colonies were picked and expanded on SNL76/7 feeder cells (ATCC, SCRC-1049) treated with mitomycin C (Sigma Aldrich) in 20% KSR medium (45). iPSCs were then transferred to feeder-free culture on Cultrex Reduced Growth Factor Basement Membrane Matrix (Trevigen)–coated plates in StemFlex medium (Thermo Fisher Scientific). Cells were passaged every 4–6 days with Versene solution (Thermo Fisher Scientific). A control iPSC line (MIN09i-33114.C) (46) was obtained from WiCell and maintained in the same way. Genotypes were matched between cells and brain tissues, with Hamming distance used to compare genomic similarity. Pluripotency of all eight lines was confirmed by TaqMan hPSC Scorecard Assay (Thermo Fisher Scientific). All lines have undergone extensive characterization for identity, pluripotency, and exogenous reprogramming factor expression (36). Genotyping with Illumina BeadChips was carried out using DNA extracted from the donors' cerebellar tissues and iPSCs. Low-quality and rare variants were removed with PLINK. For parental tissues, genotypes were prephased and imputed using genome build hg19. Short tandem repeat assay was performed using DNA extracted from dural fibroblasts and iPSCs by the Genetic Resources Core Facility at Johns Hopkins University.

Generation of Ventral Forebrain Organoids From iPSCs
To generate VFOs, iPSCs at 50%–60% confluence cultured on Cultrex-coated six-well plates in StemFlex medium were treated with 10 μM Y-27632 (BioGems) at 37°C overnight, when they reach 50%–60% confluency. The cells were then incubated with StemPro Accutase (Thermo Fisher Scientific) at 37°C for 7 minutes and dissociated into single cells. Dissociated iPSCs were plated on 96-well V-bottom plates (S-bio) at 9,000 cells/150 μL per well in StemFlex medium

with 30 μM Y-27632 and incubated at 37°C for 2 days. The StemFlex medium was gradually switched to DFN2, consisting of DMEM/F12 + GlutaMAX (Thermo Fisher Scientific) supplemented with 1× N-2 supplement (Thermo Fisher Scientific), 1× non-essential amino acids (NEAA, Thermo Fisher Scientific), 100 μM 2-mercaptoethanol (2-ME, Thermo Fisher Scientific), and 1× Antibiotic-Antimycotic (Thermo Fisher Scientific) from day 0. From day 6, the medium was gradually switched to DFN2B27, consisting of DMEM/F12 + GlutaMAX supplemented with 1× N-2 supplement, 1× NeuroCult SM1 without vitamin A (StemCell Technologies), and 1× Antibiotic-Antimycotic. On day 12, each embryoid body was embedded in a droplet of Matrigel Basement Membrane Matrix Growth Factor Reduced (Corning) as previously described (47, 48) and transferred to a 60-mm culture dish in DFN2B27. The medium was replaced on day 14. On day 16, after 4 days in static culture, the medium was switched to NBB27, consisting of Neurobasal medium (Thermo Fisher Scientific) supplemented with 1× GlutaMAX (Thermo Fisher Scientific), 1× NeuroCult SM1 (StemCell Technologies), and 1× Antibiotic-Antimycotic, and the cultures were then agitated in an incubator shaker (Eppendorf, New Brunswick S41i) at 80 rpm. The medium was supplemented with 10 μM SB 431542 (BioGems) from day 0 to day 6, 100 nM LDN-193189 (BioGems) from day 0 to day 12, 100 ng/mL human DKK-1 (PeproTech) and 0.65 μM Purmorphamine (BioGems) from day 6 to day 30, and 20 ng/mL human BDNF (PeproTech), 20 ng/mL human GDNF (PeproTech), 10 ng/mL human IGF-1 (PeproTech), and 100 μM dibutyryl-cAMP (BioGems) from day 30 to day 60. The cells were fed every 3 days from day 0 to day 60 except for day 12 and day 14. From day 60, dibutyryl-cAMP was withdrawn from the medium and the cells were fed every 3–4 days.

Real-Time qPCR
Prior to RNA extraction, organoids were minced with a blade. Total cellular RNA was extracted from small pieces of organoids using TRIzol Reagent (Thermo Fisher Scientific) and a Direct-zol RNA MiniPrep kit (Zymo Research) in accordance with the manufacturer's instructions. cDNA was prepared by reverse transcription using the SuperScript IV VILO Master Mix (Thermo Fisher Scientific). Real-time qPCR was carried out using QuantiTect SYBR Green PCR Kit (Qiagen) on QuantStudio 3 Real-Time PCR System (Applied Biosystems). The primer sequences are shown in Table S1 in the online supplement.

Immunostaining
Organoids were fixed with 4% PFA in PBS overnight at 4°C. After washing with PBS, organoids were placed in serial dilutions of PBS-buffered sucrose (10%, 20%, and 30%, in sequence) at 4°C. Each solution was replaced every day. The dehydrated organoids were maintained in 30% sucrose solution at 4°C until embedding with OCT compound (Sakura Finetek). One day before cryosectioning, fixed organoids

were placed in a 1:2 mixture of 30% sucrose solution and OCT compound and left overnight at 4°C. Organoids were then embedded in a 1:2 mixture of 30% sucrose solution and OCT compound, frozen immediately in dry ice/acetone, and cryosectioned at 10 µm. Tissue sections were washed with PBS and permeabilized and blocked with 10% normal horse serum in PBS containing 0.3% Triton X-100 for 30 minutes at room temperature. After washing with 5% serum in PBS containing 0.01% Tween-20, sections were incubated with primary antibodies at 4°C overnight and with secondary antibodies at room temperature for 2 hours. Images were analyzed using ImageJ. Detailed information regarding antibodies is available in Table S2 in the online supplement.

Western Blotting

Organoids were homogenized and lysed in RIPA buffer (150 mM NaCl, 1% NP-40, 0.5% sodium deoxycholate, 0.1% SDS, 50 mM Tris-HCl [pH 7.5]) and 1× protease inhibitor (MilliporeSigma) and centrifuged at 20,000× g for 30 minutes at 4°C. Protein concentration was measured with a BCA protein assay kit (Pierce). The whole tissue lysate and nuclei lysate were loaded onto an SDS-PAGE gel (Thermo Fisher Scientific). Signals were detected on an Odyssey DLx system (LI-COR Biosciences). Primary antibodies used for Western blotting are listed in Table S2 in the online supplement.

Multi-Electrode Array (MEA) Recording

VFOs from a control iPSC line (33114.C) were plated (one VFO per well) in 48-well MEA plates (Axion Biosystems) on day 130. The plate was coated with 0.1% polyethylenimine solution (Sigma Aldrich) and 10 µg/mL mouse Laminin (Thermo Fisher Scientific). Organoids were then fed twice a week with BrainPhys Neuronal medium (StemCell Technologies) supplemented with 1× NeuroCult SM1, 10 mM glucose, 1× Antibiotic-Antimycotic, 20 ng/mL human BDNF, 20 ng/mL human GDNF, and 10 ng/mL human IGF-1.

VFOs from four control and four schizophrenia iPSC lines were plated (one VFO per well) in 24-well MEA plates (16 electrodes per well) on day 14 and maintained in the medium described above until day 60. On day 60, the medium was switched to BrainPhys Neuronal medium. For the first 7 days, 5 µg/mL of Laminin was added to the medium to enhance the organoid attachment to the plates.

The measurements were collected 24 hours after the medium was changed, once a week, starting at 20 days after plating (150 days of organoid differentiation, control 33114.C VFO) or at day 70 of differentiation (VFOs from four control and four schizophrenia iPSC lines). Recordings were performed using a Maestro MEA system and AxIS Software Spontaneous Neural Configuration (Axion Biosystems). Spikes were detected with AxIS software using an adaptive threshold crossing set to 5.5 times the standard deviation of the estimated noise for each electrode. The plate was first allowed to rest for 3 minutes in the Maestro device, and then data were recorded for 5 minutes at 37°C and 5% CO_2. The MEA analysis was performed as previously described (49).

The pharmacological manipulation was performed with control 33114.C VFOs plated on a 48-well MEA plate (N=3–9, VFO culture), using the following compounds: 10 µM bicuculline, 50 µM muscimol, 20 µM CNQX, and 20 µM AP5. In this assessment, baseline recordings were obtained immediately before and 15 minutes after the addition of the compound(s). The organoids were washed three times with the medium, and another recording was conducted after 24 or 48 hours of incubation at 37°C in washout experiments. VFOs from four schizophrenia lines were treated with 1 µM Clozapine (MilliporeSigma) every 3 or 4 days for 2 weeks.

In Figure S6C–E in the online supplement, control VFOs were plated in high-density six-well MEA plates (one VFO per well) (MaxWell Biosystems) on day 49 inside a 5% CO_2 cell culture incubator at 37°C. Neuronal activity was recorded with a CMOS-HD-MEA system across 26,400 recording electrode sites (MaxTwo System, MaxWell Biosystems). To visualize spontaneous neuronal firing across all electrodes, an "Activity Scan Assay" was performed with MaxLab Live Software (v.20.1.6., MaxWell Biosystems) across 30 seconds using a 10-electrode configuration (see Figure S6C,D in the online supplement). A maximum distance of 100 µm was set between units. The most active 1,020 electrodes were automatically selected based on firing rates, and then recorded for at least 120 seconds ("Network Assay" in MaxLab Live). To isolate multi-unit spiking activity, resultant extracellular recordings were band-pass filtered between 300 and 4,000 Hz with a fourth-order Butterworth filter. Spikes were detected above 5.5 standard deviations, where standard deviation was estimated from the median using the Donoho formula. To account for refractory periods, spikes were detected at least 1 millisecond apart. Mean firing rate (in Hz) was calculated per organoid across all selected electrodes.

Dissociation of VFOs and Single-Cell RNA Sequencing (scRNA-seq)

Three to five VFOs were randomly selected from each iPSC line on days 70 and 150. Organoids were dissociated into single cells by using the Papain dissociation system (Worthington Biochemical) as previously described (50). To pool multiple samples together into a single library, cell hashing technology (51) was applied, in accordance with the manufacturer's instructions (BioLegend). Briefly, $1×10^6$ cells from each iPSC line were resuspended in 45 µL cell staining buffer (BioLegend) in a protein low-binding microcentrifuge tube separately and incubated with 5 µL Fc blocking reagent (BioLegend) for 10 minutes at 4°C. Precentrifuged 50 µL of hashtag antibody solution containing 2 µL of TotalSeq-A Hashtag antibody (BioLegend), with a unique barcode sequence for each iPSC line, in 48 µL cell staining buffer was added to the 50 µL blocked cell suspensions and incubated for 30 minutes at 4°C. Cells were then washed three times with cell staining buffer and resuspended in 0.4% BSA/PBS per iPSC line. Hashtagged single-cell suspension from

multiple iPSC lines (up to 12 samples) were pooled together and passed through a 35 μm filter (Falcon). Pooled cell concentration was adjusted to a density of 1,000 cells/μL 0.4% BSA/PBS, and approximately 16,000 cells were loaded onto a Chromium Single Cell 3′ Chip (10x Genomics) and 3′ gene expression libraries were generated with a Chromium Next GEM Single Cell 3′ Reagent Kits (v3.1) (10x Genomics) according to the manufacturer's instructions. Hashtag oligonucleotide (HTO) libraries were generated in accordance with BioLegend's instructions (https://www.biolegend.com/en-us/protocols/totalseq-a-antibodies-and-cell-hashing-with-10x-single-cell-3-reagent-kit-v3-3-1-protocol). Libraries were sequenced on an Illumina NovaSeq 6000 (SP, 2×50 bp) by the Genetic Resources Core Facility at Johns Hopkins University School of Medicine. HTO and 3′ gene expression libraries were sequenced on the same lane with a 1:99 ratio.

Data Analysis for scRNA-seq
Raw sequencing data were preprocessed with the Alevin software tool (v1.1.0) (52), in which reads were aligned to the hg38 human reference genome. The expression data were processed with the toolkit Scanpy (v1.7.2) (53) in Python3. Initially, cells with fewer than 200 detected genes or with mitochondrial content higher than 20% were excluded. Genes that were not expressed in at least three cells were also removed from the analysis. Read counts were normalized by counts per million in each cell and subsequently log-transformed. The most variable genes were defined as having an average normalized expression between 0.0125 and 3 and a dispersion greater than 0.5. Next, dimensionality reduction was computed by principal component analysis using the selected highly variable genes. The top 100 significant principal components were used to calculate a neighborhood graph using 15 neighbors as local size, which was then embedded in two dimensions using UMAP (uniform manifold approximation and projection). Cells were then grouped into different clusters by using the Leiden algorithm (54) with a resolution of 1.2.

A cluster of mixed neurons in VFOs was further divided into three subclusters consisting of inhibitory, excitatory, and midbrain dopaminergic (mDA) neurons with the Leiden algorithm based on the expression of specific marker genes for excitatory neurons (*SLC17A6, SLC17A7, TBR1,* and *SATB2*) and mDA neurons (*PITX3, EN1, EN2, NR4A2, DDC, SLC18A2, SLC6A3, LMX1A, LMX1B, FOXA2,* and *MSX1*). Clusters were annotated to specific cell types based on the expression patterns of known marker genes for each cell type (see Table S3 in the online supplement). Two clusters were judged to be low-quality cell clusters with a threshold of <1,000 genes detected per cell on average. These clusters were annotated as "outlier" in the set of 18 major cell types.

Differentially expressed genes (DEGs) for each cell cluster/type compared with all other cell clusters/types were found by ranking genes with the Wilcoxon rank-sum test, and the p values were adjusted for multiple testing using the Benjamini-Hochberg method. Only genes with an adjusted p value <0.05 were considered differentially expressed.

A comparison of VFO neuronal progenitor and inhibitory neuronal cell (intermediate progenitor cells [IPCs] and neurons) data to BrainSpan transcriptomic data of microdissected human brain tissue (https://www.brainspan.org/) was performed using the VoxHunt R package, with the default settings. DEGs between control and schizophrenia organoids on day 70 and day 150 in each cell type were identified by the Wilcoxon rank-sum test by considering genes that were expressed in more than 20% of cells in each iPSC line in each cell type (union of genes expressed at least 20% of cells in each iPSC lines for each cell type). Analyses were controlled for multiple testing with the Benjamini-Hochberg method. An adjusted p threshold of 0.05 was defined for statistical significance. Gene Ontology (GO) enrichment and Kyoto Encyclopedia of Genes and Genomes (KEGG) enrichment of DEGs were performed using the g:Profiler package (55). Enrichment analysis with GWAS-significant genes (3) and transcriptome-wide association study (TWAS)–significant and differentially expressed genes in postmortem caudate tissue (38) and cortical tissue (56) from individuals with schizophrenia was performed with Fisher's exact test.

Trajectory Analysis
RNA velocity analysis (57) on neuronal progenitors (radial glia [RG], ventral RG, and outer RG), inhibitory IPC, and inhibitory neurons in VFOs was performed using the scVelo (v.0.2.4) Python package (58) using a dynamical model with differential kinetic analysis. The number of spliced and unspliced reads was counted directly on the Alevin output. Genes with fewer than 20 counts (for both unspliced and spliced) were filtered out, whereas all DEGs identified in neuronal progenitors and inhibitory neurons were retained. The 10,000 most variable genes were then used for the next steps. Count normalization, computation of first- and second-order moments, velocities estimation, and UMAP embedding were all performed with the default parameters of the built-in functions (https://scvelo.readthedocs.io/). Potential driver genes and latent time were also computed with default parameters. Differences in the distribution of each cell type across latent time between control and schizophrenia iPSC lines were performed using the Kolmogorov-Smirnov test. Enrichment of driver genes with DEGs in each cell type of VFOs and schizophrenia risk genes (3, 38, 56) was calculated with Fisher's exact test.

Fuzzy c-Mean Analysis
Fuzzy c-mean clustering was performed using the R package Mfuzz (v2.54.0) (59) on the human LGE scRNA-seq preprocessed data kindly provided by Bocchi et al. (60). Briefly, pseudo-bulk gene expression was created from a normalized single-cell gene expression matrix for each cell type according to fetal age (postconception weeks 7, 9, and 11). We then standardized and clustered each group of pseudo-bulk

gene expression by cell type and fetal age in 10 modules. Cluster plots were created using the mfuzz.plot function.

Statistics

Data are presented as mean and standard deviation or mean and standard error of the mean. Box plots show maximum, third quartile, median, first quartile, and minimum values. Raw data were tested for normality of distribution, and statistical analyses were performed with unpaired t tests (two-tailed), Mann-Whitney U tests, one-way analysis of variance tests with post hoc multiple comparisons, or Kruskal-Wallis tests with post hoc multiple comparisons, using GraphPad Prism (version 7). A p value <0.05 was considered to indicate a significant difference between groups.

RESULTS

Generation and Characterization of iPSC-Derived Ventral Forebrain Organoids

To investigate striatal neurodevelopmental origins of schizophrenia with brain organoids and explore how the iPSC-based model can recapitulate pathophysiological changes observed in adult patient brains, we first established iPSCs from neurotypical control individuals and individuals with schizophrenia whose genotypic and transcriptomic data of postmortem brain tissue are available through the BrainSeq neurogenomics consortium (61). To maximize genetic risk differences between controls and patients, we selected iPSC donors with nonoverlapping schizophrenia PRSs between the groups: four control individuals whose PRSs were among the lowest and four schizophrenia individuals with high PRSs in the postmortem brain cohort (Figure 1A; see also Figure S1A in the online supplement). We then reprogrammed postmortem dura-derived fibroblasts from these eight individuals into iPSCs and confirmed their pluripotency, no genomic insertion of episomal vectors or SeV used for reprogramming, and genotype matching with donor brains and with donor fibroblasts (see Figure S1B–H in the online supplement) (36).

Given the subpallial origin of striatal neurons (Figure 1B), we developed a protocol for differentiation of iPSCs into VFOs to simulate the human striatum development by ventralizing neural cells with DKK-1, a Wnt signaling pathway inhibitor, and sonic hedgehog agonist purmorphamine (Figure 1C). On day 12, VFOs showed suppression of the pluripotent stem cell marker *OCT4/POU5F1*, and upregulation of genes that represent induction of neural fate and differentiation of the ventral and dorsal forebrain, compared with undifferentiated iPSCs (see Figure S2A in the online supplement). In addition, VFOs on day 12 started expressing LGE, MGE, CGE, and neocortex marker genes. On day 37, more mature marker genes for these brain regions were expressed in the VFOs. No differences were observed between control- and schizophrenia-derived VFOs except in the expression of *POU5F1*, suggesting no difference in the response to VFO differentiation factors between the groups,

at least during very early neuronal induction (see Figure S2A in the online supplement). By day 37, VFOs exhibited ventricular zone-like structures consisting of Ki67-positive proliferative neural progenitor cells around the ventricles labeled with ZO-1 (Figure 1D). We found that SOX2-expressing neural progenitor cells within these structures expressed markers for the LGE (MEIS2), MGE (NKX2-1), and CGE (COUP-TFII) (Figure 1E; see also Figure S2B in the online supplement).

To profile cellular diversity in the VFOs, we performed scRNA-seq analysis on day 70 and day 150 (N=15,424 cells from four control and three schizophrenia iPSC lines) (see Table S4 in the online supplement). Clustering by Leiden algorithm (54) combined with guide subclustering identified 27 clusters in VFOs, which were then annotated based on the number of genes detected, for defining low-quality cell clusters, and according to the similarity to cell clusters in cerebral organoids from a recent study (62) (see Figure S2C–E in the online supplement). We then further annotated 27 clusters into 18 major cell types (Figure 1F) based on the expression of known marker genes (see Figure S3A and Table S3 in the online supplement) and validated the annotation by comparing the gene expression profiles of each cell type in VFOs with recently published cell types in brain organoids (60, 63, 64) (see Figure S3B–D in the online supplement). The 18 cell types consisted of cells such as inhibitory and excitatory IPCs and neurons; neuronal progenitors such as RG and outer RG; and non-neuronal cells such as astrocytes and choroid plexus cells (Figure 1F,G). Among IPCs and neurons, 67.4% of cells were inhibitory population, and the remaining 32.6% were excitatory IPCs/neurons (14.6%), mDA neurons (11.5%), and Cajal-Retzius cells (6.5%), indicating the ventralized neuronal lineage in VFOs (Figure 1G).

Inhibitory Neuronal Populations in VFOs Represent the Cell Identities of Immature Striatal Neurons

Because in the present study we sought to investigate the neurodevelopmental underpinnings of altered striatal function in the pathogenesis of schizophrenia, we further characterized neuronal progenitors and inhibitory IPCs and inhibitory neurons (Figure 1H; see also Figure S4A,B in the online supplement).

Neuronal progenitors including RG, outer RG, and ventral RG, which we will refer to as progenitors, expressed marker genes for the ventricular zone of the human subpallium at gestational weeks 9–12 (65) (see Figure S4C in the online supplement). By contrast, inhibitory IPCs were positive for subventricular zone markers, while inhibitory neurons showed low expression of these ventricular and subventricular zone markers (65) (see Figure S4C). Progenitors showed the highest similarity to ganglionic eminences, the origin of striatal inhibitory neurons, at postconception weeks 8–9 (Figure 1I), and inhibitory IPCs and neurons showed the highest similarity to the striatum at postconception weeks 12–16 (Figure 1J) when compared with human fetal brain samples from the BrainSpan human transcriptomic data set

with the VoxHunt algorithm (66). Additionally, we found that inhibitory neurons expressed genes that were upregulated in the human LGE at later developmental stages (60) compared with progenitors and inhibitory IPCs (Figure 1K). Moreover, the gene expression patterns of progenitors showed higher similarity to progenitor populations than neuronal populations in the human developing striatum (60), while inhibitory neurons were more similar to neuronal populations (Figure 1L).

We confirmed the expression of representative marker genes for the MGE, LGE, and CGE in progenitors and the inhibitory neuronal population (see Figure S4D–G in the online supplement). A recent study demonstrated that the expression of *NR2F1* and *NR2F2*, which are defined markers for the CGE in rodents, was detected in the MGE and LGE as well as the CGE in the human subpallium (41). Given that only a few cells express other CGE-specific marker genes (*SP9*, *SP8*, and *CALB2*) (see Figure S4D,G in the online supplement), our analysis suggests that neuronal cells in VFOs are composed of cells with all three ganglionic eminence lineages, despite high levels of *NR2F1* and *NR2F2* expression.

Consistent with the similarity to the human developing striatum (Figure 1J), inhibitory neurons in VFOs expressed marker genes for both pre-MSNs, such as *MEIS2* and *POU3F1*, and MSNs, such as *FOXP2*, *ARPP21*, and *CALB1* (see Figure S4H–J in the online supplement). We observed the expression of marker genes such as *TAC1* and *EBF1* for pre-MSNs with D_1 dopamine receptors (pre-D1 MSNs) and *SIX3* and *GRIK3* for pre-MSNs with D_2 dopamine receptors (pre-D2 MSNs) (see Figure S4H,K,L in the online supplement). Marker genes for MSN subtypes at mature stages, including *IKZF1*, *PDYN*, *DRD1* (D1 MSNs) and *EGR3*, *PENK*, *ADORA2A*, *DRD2* (D2 MSNs), were rarely detected in inhibitory neurons in VFOs (see Figure S4H in the online supplement). These gene expression patterns suggest that inhibitory neurons in VFOs had MSN fate but were still at an immature stage of human striatal development.

In addition to MSNs, ganglionic eminences give rise to both striatal and cortical interneurons. We found more cells expressing marker genes specific to striatal interneurons (*EPHB1*, *NKX2-1*, and *EPHB3*) than markers for cortical interneurons (*NRP1*, *RELN*, *LHX6*, and *HTR3A*) among inhibitory neurons in VFOs (see Figure S4M–O in the online supplement). A small percentage of inhibitory neurons expressed the subtype-specific striatal GABAergic interneuron marker *CALB2*, but we found only very few cells expressing other subtype-specific markers, such as *SST*, *NOS1*, *NPY*, *TH*, *CCK*, *VIP*, *TAC3*, *PVALB*, and *PTHLH* (see Figure S4M,P in the online supplement), suggesting that GABAergic interneurons in VFOs are also at an immature stage. We found very few cholinergic cells among inhibitory neurons in VFOs (see Figure S4M,Q in the online supplement). Furthermore, inhibitory neurons in VFOs expressed marker genes for the striosome and the matrix (see Figure S4R,S in the online supplement), the two compartments in the striatum defined by their gene expression profiles and histology (67, 68).

As we found no unique cell type restricted to day 70 or day 150 (see Figure S5A,B in the online supplement), we decided to pool the cells from the two time points together for further analyses. DEGs between the two time points, however, indicated that neurons in 150-day-old VFOs were more mature than neurons in 70-day-old VFOs, with upregulated synaptic genes and downregulated expression of ribosomal genes (see Figure S5C–G and Table S5 in the online supplement).

In summary, we established a protocol for the differentiation of VFOs from iPSCs and validated the developing human striatal identity of inhibitory neuronal cells in VFOs.
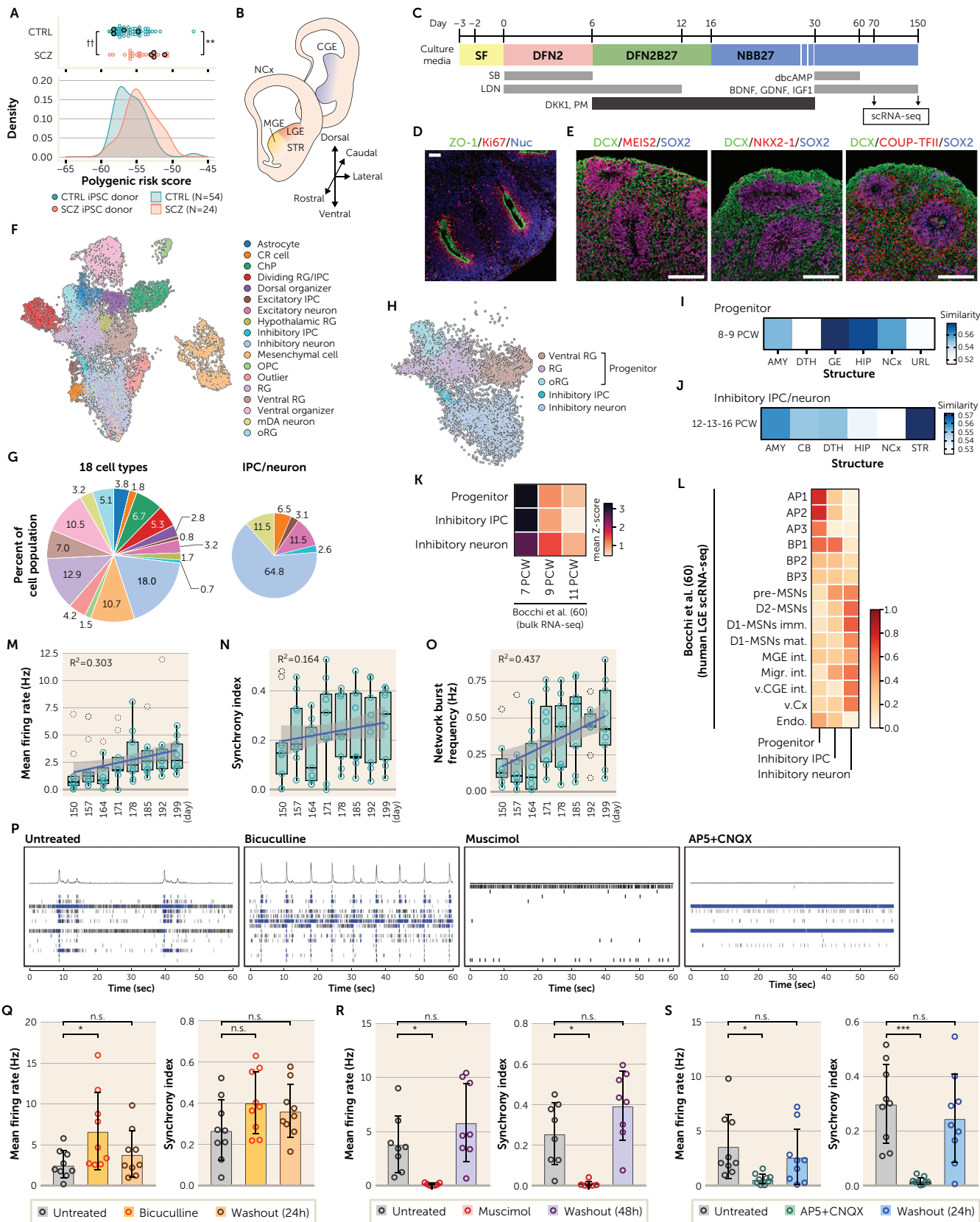
VFOs Form Functional Neural Circuits

To evaluate the functionality of VFOs, we performed extracellular recording of spontaneous electrical activity using MEAs in VFOs from a control individual (33114.C). We first observed a consistent increase in mean firing rate ($R^2=0.303$) (Figure 1M), synchrony index ($R^2=0.164$) (Figure 1N), and network burst frequency ($R^2=0.437$) (Figure 1O) across days of organoid maturation (at days 150–199), in addition to consistent increases in the number of bursts ($R^2=0.445$) and network bursts ($R^2=0.479$) per minute (see Figure S6A,B in the online supplement), which indicates continuous maturation of neuronal networks. With high-density MEA (MaxWell Biosystems), we confirmed that the increases in neuronal activity and network formation across days in vitro were mainly related to neuronal maturation in VFOs, but not to structural changes of the stationary organoids on the electrodes, as mean firing rate increased regardless of the increase in area covered by flattened organoid or axons migrated out from the organoid (see Figure S6C–E in the online supplement).

We then evaluated the role of inhibitory and excitatory synaptic transmissions in functional network activity by pharmacological intervention (Figure 1P). The spontaneous neuronal firing and synchronized bursting were increased by the GABA$_A$ receptor antagonist bicuculline (Figure 1Q; see also Figure S6F in the online supplement) and were blocked by both the GABA$_A$ receptor agonist muscimol and glutamate receptor antagonists (AP5 and CNQX) (Figure 1R,S; see also Figure S6G,H in the online supplement).

Since GABAergic neurons are known to be excitatory during early brain development and switch their mode of synaptic transmission to inhibitory upon maturation (69), we validated the expression of *SLC12A2* (also known as *NKCC1*) and *SLC12A5* (*KCC2*), which encode cation-chloride cotransporters that regulate the excitatory-inhibitory transition. Inhibitory neurons in VFOs expressed both of the cotransporters. However, the expression of *SLC12A5* was higher than that of *SLC12A2*, suggesting that inhibitory neurons in VFOs contribute to the inhibitory synaptic transmission (see Figure S7A in the online supplement). Additionally, neurons in VFOs expressed genes encoding

FIGURE 1. Generation and characterization of iPSC-derived ventral forebrain organoids[a]

[a] Panel A presents plots of schizophrenia polygenic risk scores based on a recent genome-wide association study (3) in the dural fibroblast cohort including four control individuals (CTRL) and four individuals with schizophrenia (SCZ) analyzed in this study. iPSC=induced pluripotent stem cell. ††p=0.0083, Mann-Whitney U test (54 CTRL vs. 24 SCZ); **p=0.0021, unpaired t test (four CTRL vs. four SCZ). Panel B is a schematic of the human

target receptor subunits for each pharmacological intervention (see Figure S7B–E in the online supplement). We confirmed the differences in the expression of NKCC1 and KCC2 and of NMDAR2A and NMDAR2B in VFOs at the protein level (see Figure S7F,G in the online supplement). VFOs expressed KCC2 and NMDAR2B more than NKCC1 and NMDAR2A, respectively. We also observed KCC2-expressing neurons in VFOs from both the control and schizophrenia lines (see Figure S7H in the online supplement).

These data suggest that VFOs have intrinsic GABAergic and glutamatergic synaptic transmissions, in which GABAergic neurons modulate neuronal activity suppressively. In summary, we successfully generated VFOs enriched for functional inhibitory neurons showing immature striatal properties.

Schizophrenia VFOs Do Not Exhibit Structural Differences Compared With Control VFOs
Using the VFO model of human striatal development to understand the neurodevelopmental mechanisms underlying the striatal pathogenesis of schizophrenia, we next investigated structural differences in VFOs derived from four control individuals and three individuals with schizophrenia. We first compared the cell type composition of control- and schizophrenia-derived VFOs by scRNA-seq at day 70 and day 150 of differentiation (Figure 2A). The quality of the sequenced cells, evaluated by total UMI counts, number of genes detected, and percentage of mitochondrial genes per cell, did not differ between the groups (see Table S6 in the online supplement). Of note, consistent with previous reports demonstrating variance driven by the genetic background of an iPSC line (70, 71), we found considerable variety in the cell type composition of VFOs generated from the cohort of iPSC lines regardless of whether they were from the control or schizophrenia individuals (see Figure S8A–E and Table S7 in the online supplement). However, we did not observe significant differences in VFO (days 70 and 150) cell type composition between the control and

schizophrenia iPSC lines, except for mesenchymal cells and RG (Figure 2B), with the differences driven by VFOs at day 70 (see Figure S8F in the online supplement).

To explore structural differences in inhibitory neuronal populations between the groups, we performed immunostaining of VFOs. On day 70, VFOs from both the control and schizophrenia individuals had ventricular zone-like structures (Figure 2C), and the thickness of SOX2-expressing (SOX2$^+$) neural progenitor cell layers in the ventricular zone structure did not differ between the groups (Figure 2D). This structure disappeared by day 160 as both groups of VFOs matured (see Figure S9A in the online supplement), but still comparable areas of SOX2$^+$ neural progenitor cells (see Figure S9B in the online supplement). Additionally, we did not find differences between the groups in the pre-MSN population expressing MEIS2 or FOXP2 on day 70 (Figure 2E,F), GABAergic neurons (Figure 2G,H), and DARPP32$^+$ MSNs (Figure 2I,J) on day 160. In addition to MSNs, we found GABAergic striatal interneurons expressing calretinin (Figure 2I), consistent with the expression of CALB2 in scRNA-seq (see Figure S4M,P in the online supplement). Moreover, we found astrocytes expressing GFAP and/or S100B (see Figure S9C in the online supplement). This cell type became abundant on day 150 compared with day 70 (see Figure S5B in the online supplement). We did not observe a difference in GFAP intensity between control and schizophrenia VFOs (see Figure S9D in the online supplement).
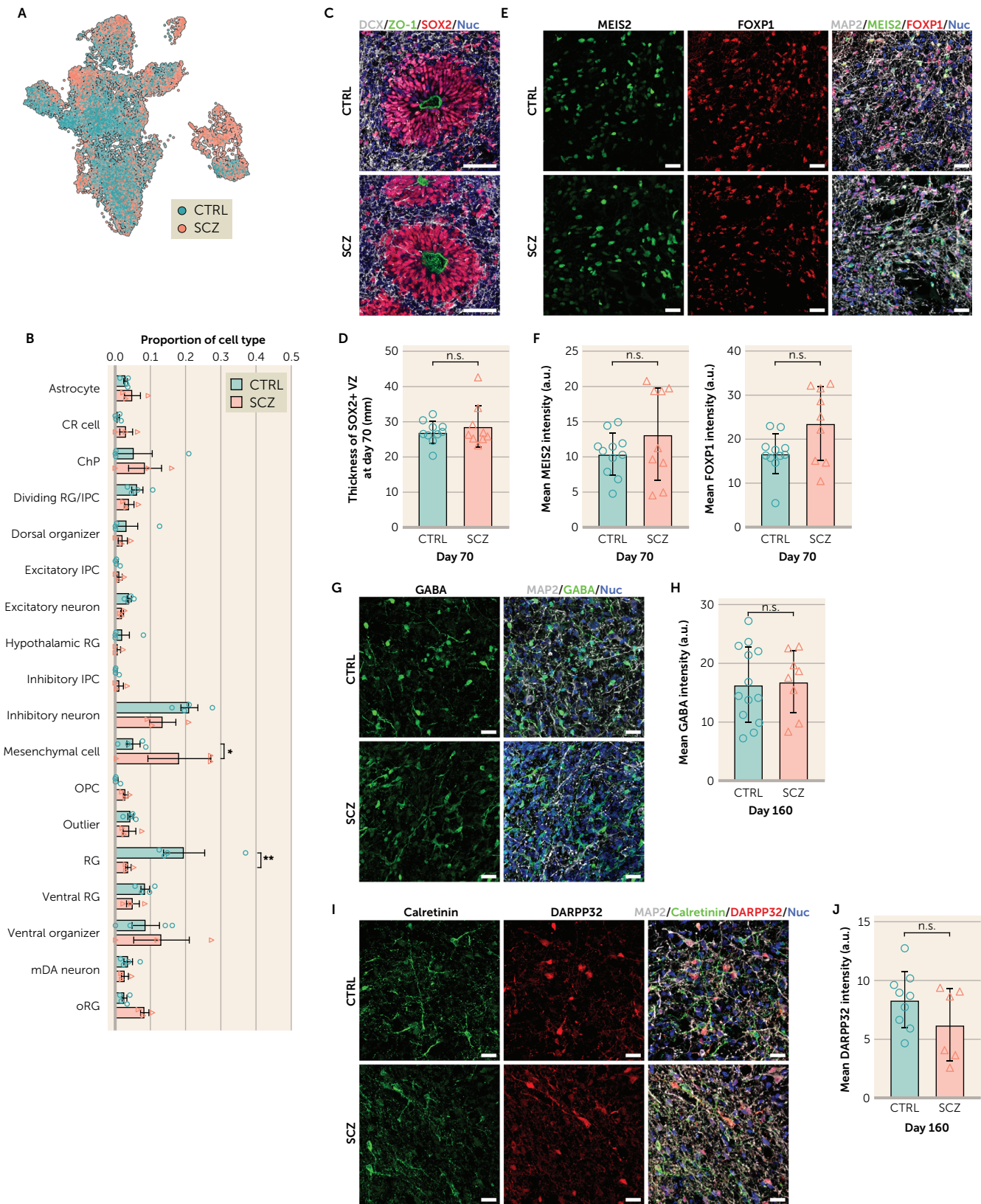
We have shown that there were no significant structural differences between VFOs derived from control individuals and VFOs derived from individuals with schizophrenia.

Transcriptional Differences Suggest Accelerated Differentiation of Striatal Neurons in Schizophrenia
We next sought to investigate transcriptional differences in VFOs between the groups. To understand the

developing brain. CGE=caudal ganglionic eminence; LGE=lateral ganglionic eminence; MGE=medial ganglionic eminence; NCx=neocortex; STR=striatum. Panel C is a schematic protocol for generation of ventral forebrain organoids (VFOs). BDNF=brain-derived neurotrophic factor; dbcAMP=dibutyryl cyclic-AMP; DKK1=dickkopf-related protein 1; GDNF=glial cell–derived neurotrophic factor; IGF1=insulin growth factor-1; LDN=LDN-193189; PM=purmorphamine; SB=SB431542. Panels D and E show representative immunostaining of VFOs derived from control individuals (LIBD7c6 and LIBD2c1, respectively) on day 37 and day 30, respectively. Nuclei in panel D are stained by Hoechst 33342 (blue). Scale bars are 50 μm in panel D and 100 μm in panel E. Panel F is a UMAP (uniform manifold approximation and projection) showing 15,424 cells from VFOs of four CTRL and three SCZ individuals on days 70 and 150, colored by 18 major cell types. ChP=choroid plexus; CR cell=Cajal-Retzius cell; IPC=intermediate progenitor cell; mDA neuron=midbrain dopaminergic neuron; OPC=oligodendrocyte progenitor cell; oRG=outer radial glia; RG=radial glia. Panel G shows the composition of all 18 major cell types and of six major cell types among the IPC/neuron population in VFOs from seven individuals (four CTRL and three SCZ). Panel H is a UMAP of progenitors including ventral RG, RG, and oRG and inhibitory neuronal population in VFOs (6,747 cells) from four CTRL and three SCZ individuals, colored by major cell type. Panels I and J are heat maps showing gene expression similarity of progenitors in VFOs to the BrainSpan data set at postconception weeks (PCW) 8 and 9 (panel I) and similarity of inhibitory IPC/neurons in VFOs to the BrainSpan data set at PCW 12, 13, and 16 (panel J). AMY=amygdala; CB=cerebellum; DTH=dorsal thalamus; GE=ganglionic eminence; HIP=hippocampus; NCx=neocortex; STR=striatum; URL=upper (rostral) rhombic lip. Panel K is a matrix plot showing expression of genes upregulated in human LGE at PCW 7, 9, and 11 compared with MGE and neocortex (60) in inhibitory neuronal cells in VFOs from four CTRL and three SCZ individuals. Panel L is a heat map showing overlap of differentially expressed genes in each inhibitory neuronal cell type compared with all other cell types in VFOs with cell type–specific genes in single-cell RNA sequencing of human LGE (PCW 7–11) (60). The color indicates the overlap coefficient. Panels M–O show time series of mean firing rate, synchrony index, and network burst frequency, respectively, of VFOs derived from a control individual (33114.c) between day 150 and day 199 (N=3–9; VFOs for each time point). Dashed circles indicate outliers. Panel P shows representative raster plots of untreated and control VFOs (33114.c) treated with bicuculline, muscimol, or AP5+CNQX at days 220–241. Panels Q–S show the effect of treatments with bicuculline, muscimol, and AP5+CNQX, respectively, on mean firing rate and synchrony index of control VFOs (33114.c) at days 220, 241, and 227, respectively. *p<0.05; ***p<0.001; n.s.=not significant; one-way analysis of variance with post hoc Tukey's multiple comparisons test. Outliers were removed on Prism with ROUT (Q=1%). Error bars indicate standard deviation. (N=7–9; VFOs for recording.)

FIGURE 2. No structural differences between control- and schizophrenia-derived ventral forebrain organoids[a]

[a] Panel A is a UMAP (uniform manifold approximation and projection) showing 15,424 cells from ventral forebrain organoids (VFOs) from four control individuals (CTRL) and three individuals with schizophrenia (SCZ) on days 70 and 150, colored by diagnosis. Panel B shows the mean proportions of 18 major cell types in VFOs from four CTRL and three SCZ individuals (day 70 + day 150). Error bars indicate standard error of the mean. *p=0.0304, **p=0.0029, two-way analysis of variance with post hoc Bonferroni multiple comparisons test. CR cell=Cajal-Retzius cell; ChP=choroid plexus;

neurodevelopmental molecular underpinnings of the striatal pathogenesis of schizophrenia, we explored differences in gene expression patterns between VFOs derived from control (N=4) and schizophrenia (N=3) lines in the cell types primarily associated with the ganglionic eminence and/or striatum: progenitors and inhibitory neurons (Figure 1I–L and Figure 3A–D). Of note, we excluded inhibitory IPCs from the analysis, as the majority of this population was represented in only two iPSC lines (see Figure S8E and Table S7 in the online supplement). We confirmed that the progenitor proportion as well as inhibitory neurons did not differ between the groups (Figure 3E). Additionally, neither of these populations was driven disproportionately by a specific iPSC line (progenitor cell count: control VFOs, 686 [SD=225.55]; schizophrenia VFOs, 370 [SD=36.17]; progenitor cell proportion: control VFOs, 0.31 [SD=0.11]; schizophrenia VFOs, 0.17 [SD=0.01]; inhibitory neuron cell count: control VFOs, 482 [SD=150.88]; schizophrenia VFOs, 285 [SD=94.98]; inhibitory neuron cell proportion: control VFOs, 0.21 [SD=0.04]; schizophrenia VFOs, 0.14 [SD=0.05]).

We identified 575 genes that were significantly differentially expressed in progenitors between the groups, of which 243 genes were upregulated and 332 were downregulated in schizophrenia VFOs (Figure 3F; see also Table S8 in the online supplement). These DEGs included several GWAS-significant genes (3), such as *CLU*, *GPM6A*, *EGR1*, *NMB*, *MAPT*, *SOX2-OT*, and *PSMA4* (Figure 3F,G). We also found cycline genes such as *CCND1* among the genes downregulated in schizophrenia VFOs (Figure 3F,G).

In inhibitory neurons, 144 genes were significantly differentially expressed between control and schizophrenia VFOs (Figure 3H; see also Table S8 in the online supplement). Of these 144 DEGs, 45 genes were upregulated and 99 were downregulated in inhibitory neurons derived from individuals with schizophrenia compared with controls. There were synaptic genes such as *NRXN1* among the upregulated genes (Figure 3H,I). We also identified genes such as *CRABP1*, *POU3F2*, and *NOVA1*, whose dysregulation has been linked to schizophrenia risk (72–75), among the downregulated genes (Figure 3H,I).

GO analysis revealed significant upregulation of neurogenic processes and marked downregulation of the mitotic cell cycle in progenitors in schizophrenia VFOs compared with control VFOs (Figure 3J; see also Table S9 in the online supplement). Notably, synaptic signaling-related processes were upregulated and translation-related processes were remarkably downregulated in schizophrenia VFOs for both progenitors and inhibitory neurons compared with control VFOs (Figure 3J,K; see also Table S9 in the online supplement). Previous studies have demonstrated the global increase in translation upon neuronal differentiation and the global decrease as neurons mature (76, 77). Overall, these results suggest accelerated differentiation of striatal neuronal cells in VFOs from individuals with schizophrenia compared with control VFOs.
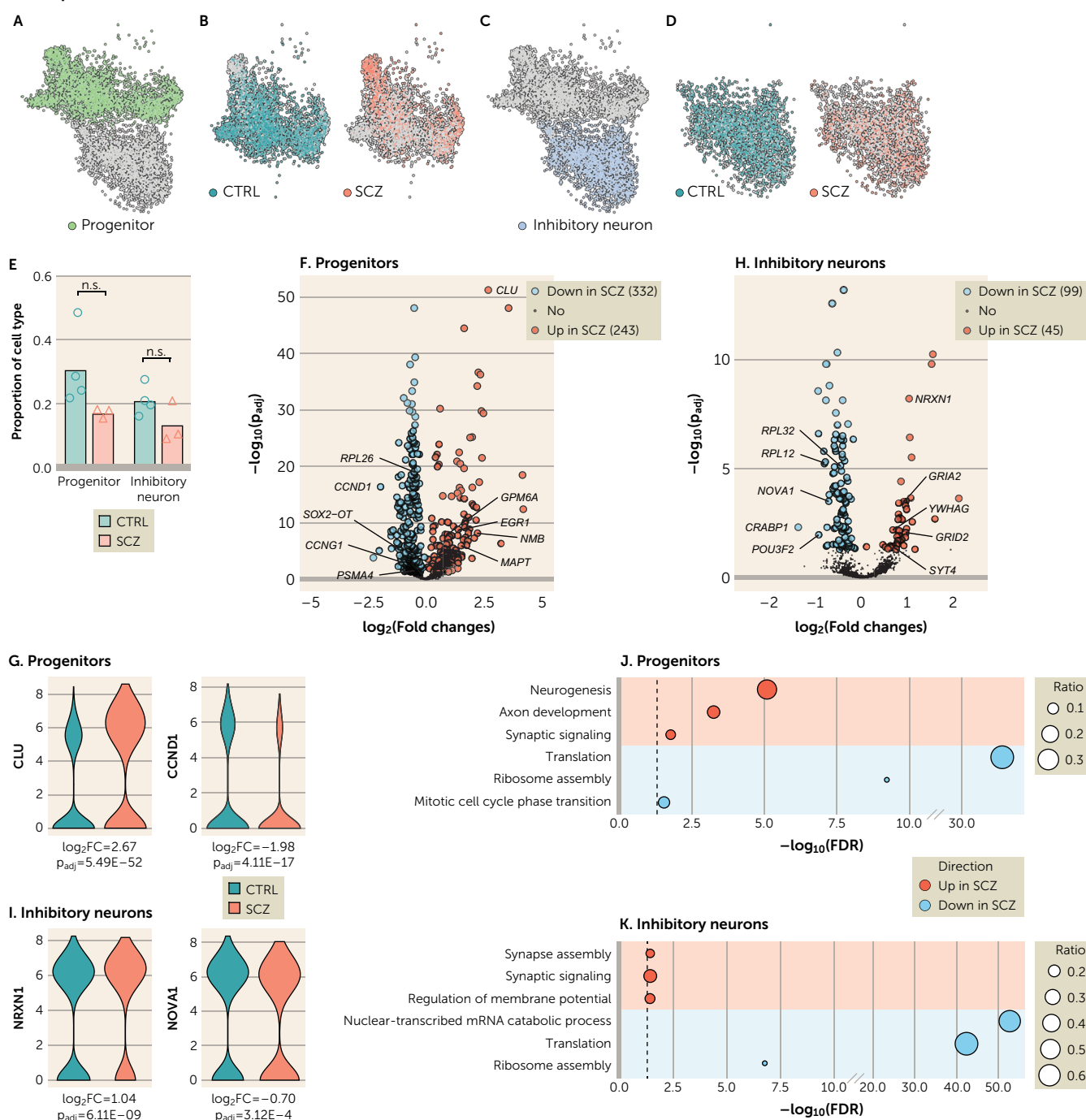
Striatal Inhibitory Neuronal Cells Exhibit Accelerated Differentiation in Schizophrenia VFOs Compared With Control VFOs

The findings of accelerated differentiation of striatal neuronal cells in schizophrenia VFOs led us to further investigate differences in the developmental trajectories of striatal inhibitory neuronal cells between control and schizophrenia VFOs by RNA velocity analysis (57, 58). The velocity field map of the inhibitory neuronal population, including progenitors, IPCs, and neurons, reflected the dynamics of neuronal differentiation as these cells transition from ventral RG or RG to neurons, with or without passing through outer RG or IPC phases (Figure 4A; see also Figure S10A in the online supplement). The inferred latent time also demonstrated the neurodevelopmental trajectory, in which progenitors and IPCs were both produced earlier than neurons (Figure 4B,C; see also Figure S10B in the online supplement).

Consistent with transcriptional differences indicating accelerated differentiation, we found that both progenitors and inhibitory neurons in schizophrenia VFOs have more cells at later developmental stages compared with these populations in control VFOs, based on the latent time (Figure 4D). These findings further indicate the promoted developmental state of the inhibitory neuronal population in VFOs derived from individuals with schizophrenia compared with VFOs from control individuals.

The RNA velocity analysis also identified putative driver genes of transcriptional changes in each cell type, such as *PTN* for progenitors and *NEDD4L* for inhibitory neurons

---

RG=radial glia; IPC=intermediate progenitor cell; OPC=oligodendrocyte progenitor cell; mDA neuron=midbrain dopaminergic neuron; oRG=outer RG. Panel C shows representative immunostaining images of VFOs derived from CTRL (LIBD9c1) and SCZ (LIBD8c4) individuals at day 70, showing SOX2$^+$ ventricular zone. Nuclei are stained by Hoechst 33342 (blue). Scale bars, 50 μm. Panel D shows the quantification of thickness of SOX2$^+$ ventricular zone (VZ) in VFOs at day 70 (N=4 CTRL lines; N=3 SCZ lines; 2–3 organoids per line). n.s.=not significant, Mann-Whitney U test. Averages of 7–93 structures per organoid were analyzed. Panel E shows representative immunostaining images of VFOs derived from CTRL (LIBD2c1) and SCZ (LIBD5c7) individuals at day 70, showing pre-MSN/MSN (medium spiny neurons) expressing MEIS2 and/or FOXP1. Nuclei are stained by Hoechst 33342 (blue). Scale bars, 20 μm. Panel F shows the quantification of mean intensity of MEIS2 and FOXP1 in VFOs at day 70 (N=4 CTRL lines; N=3 SCZ lines; 2–3 organoids per line). n.s.=not significant, unpaired t test. Panel G shows representative immunostaining images of VFOs derived from CTRL (LIBD2c1) and SCZ (LIBD8c4) individuals at day 160, showing GABAergic neurons. Nuclei are stained by Hoechst 33342 (blue). Scale bars, 20 μm. Panel H shows the quantification of mean intensity of GABA in VFOs at day 160 (N=4 CTRL lines; N=3 SCZ lines; 2–3 organoids per line). n.s.=not significant, unpaired t test. Panel I shows representative immunostaining images of VFOs derived from CTRL (LIBD2c1) and SCZ (LIBD5c7) individuals at day 160, showing calretinin$^+$ striatal interneurons and DARPP32$^+$ MSNs. Nuclei are stained by Hoechst 33342 (blue). Scale bars, 20 μm. Panel J shows the quantification of mean intensity of DARPP32 in VFOs at day 160 (N=4 CTRL lines; N=3 SCZ lines; 2–3 organoids per line). n.s.=not significant, unpaired t test. Error bars in graphs indicate standard deviation.

FIGURE 3. Transcriptional differences in striatal inhibitory neuronal cells of ventral forebrain organoids between control and schizophrenia lines[a]

[a] Panel A is a UMAP (uniform manifold approximation and projection) of inhibitory neuronal cells (progenitor, inhibitory IPC, and inhibitory neuron) from ventral forebrain organoids (VFOs) of four control (CTRL) and three schizophrenia (SCZ) lines on days 70 and 150. Progenitors are highlighted in light green. Panel B is a UMAP of progenitors from VFOs of four CTRL and three SCZ lines on days 70 and 150. Cells belonging to CTRL and SCZ lines are visualized individually. Panel C is a UMAP of inhibitory neuronal cells from VFOs of four CTRL and three SCZ lines on days 70 and 150. Inhibitory neurons are highlighted in light blue. Panel D is a UMAP of inhibitory neurons from VFOs of four CTRL and three SCZ lines on days 70 and 150. Cells belonging to CTRL and SCZ lines are visualized individually. Panel E shows a comparison of proportion of progenitor and inhibitory neuron between four CTRL and three SCZ lines (days 70 and 150). n.s.=not significant, unpaired t test. Panel F is a volcano plot showing differentially expressed genes (DEGs) in progenitors between CTRL and SCZ lines. p_{adj}=adjusted p value. Schizophrenia genome-wide association study–significant genes (*CLU*, *GPM6A*, *EGR1*, *NMB*, *MAPT*, *SOX2-OT*, *PSMA4*) (3), a ribosomal gene (*RPL26*), and cell cycle-associated genes (*CCND1* and *CCNG1*) were labeled. Panel G shows representative genes upregulated (*CLU*) and downregulated (*CCND1*) in SCZ progenitors compared with CTRL progenitors. FC=fold change. Panel H is a volcano plot showing DEGs in inhibitory neurons between CTRL and SCZ lines. Synaptic genes (*NRXN1*, *GRIA2*, *YWHAG*, *GRID2*, and *SYT4*), ribosomal genes (*RPL12* and *RPL32*), and schizophrenia-associated genes (*NOVA1*, *CRABP1*, and *POU3F2*) were labeled. Panel I shows representative genes upregulated (*NRXN1*) and downregulated (*NOVA1*) in SCZ inhibitory neurons compared with CTRL inhibitory neurons. Panel J is a dot plot showing

(see Figure S10C,D and Table S10 in the online supplement). Driver genes display pronounced dynamic behavior and are involved in directing lineage fate decisions. We found significant overlap between driver genes and upregulated genes in schizophrenia in both progenitors and inhibitory neurons (Figure 4E; see also Table S11 in the online supplement), supporting the accelerated differentiation phenotype of striatal neuronal cells derived from individuals with schizophrenia.

Interestingly, driver genes for progenitors significantly overlapped with schizophrenia TWAS-significant genes in postmortem caudate tissue (see Figure S10E and Table S12 in the online supplement). Moreover, driver genes for inhibitory neurons showed substantial overlap with the TWAS genes in caudate and schizophrenia GWAS-significant genes (see Figure S10E and Table S12 in the online supplement). Of note, driver genes for progenitors and inhibitory neurons do not overlap with schizophrenia TWAS-significant genes found in postmortem dorsolateral prefrontal cortex (DLPFC) (see Figure S10E and Table S12 in the online supplement). These findings suggest that alterations of cell type–specific key genes that regulate the transcriptomic dynamics of striatal neuronal differentiation contribute to schizophrenia pathogenesis, and particularly to aberrant striatal function in schizophrenia.

To assess whether our findings of differences in the striatal differentiation of VFOs between control and schizophrenia VFOs are relevant to physiological maturation patterns, we compared gene expression patterns in inhibitory neuronal cells in VFOs to developing human striatal transcriptome data (60). As shown in Figure 1K, inhibitory neuronal cells in VFOs seemed to follow the maturation patterns of the developing human striatum. Both progenitors and inhibitory neurons in schizophrenia-derived VFOs displayed increased expression of genes known to be highly expressed at later stages of human striatal development compared with control VFOs (60) (Figure 4F), suggesting promoted striatal differentiation in schizophrenia VFOs. We further investigated the expression patterns of genes that exhibited continuous upregulation in progenitors and neurons in the developing human striatum (60) in inhibitory neuronal populations in VFOs, using fuzzy c-mean clustering (59). Progenitors in schizophrenia VFOs showed higher expression of genes that are continuously upregulated in progenitors in the developing human striatum than did progenitors in control VFOs (Figure 4G,H; see also Figure S11A in the online supplement). These genes included, for example, *SLC1A3*, *NFIA*, *NTRK2*, and *SLC4A4*, which were also identified as putative driver genes for progenitors in VFOs (Figure 4I). In addition, continuously upregulated genes in MSNs of the developing human striatum (60) were

highly expressed in inhibitory neurons of schizophrenia VFOs compared with control VFOs (Figure 4J,K; see also Figure S11B in the online supplement). These genes included driver genes for inhibitory neurons such as *SCN3B*, *MAPT*, *RTN1*, and *CELF4* (Figure 4L).

We have demonstrated that inhibitory neuronal cells mature at a faster rate in schizophrenia VFOs than in control VFOs. Given that we did not observe a difference in the cell type proportions of VFOs at day 70 and day 150 between the control and schizophrenia groups (see Figure S11C in the online supplement), we excluded the possibility that the differences in neurodevelopmental trajectory arose from the difference in the experimental age of the cells. In summary, our findings from cell type–specific analyses of the VFO model of human striatal development support the acceleration of inhibitory neuronal differentiation in the striatal developmental trajectory as a molecular underpinning of the striatal pathogenesis of schizophrenia.
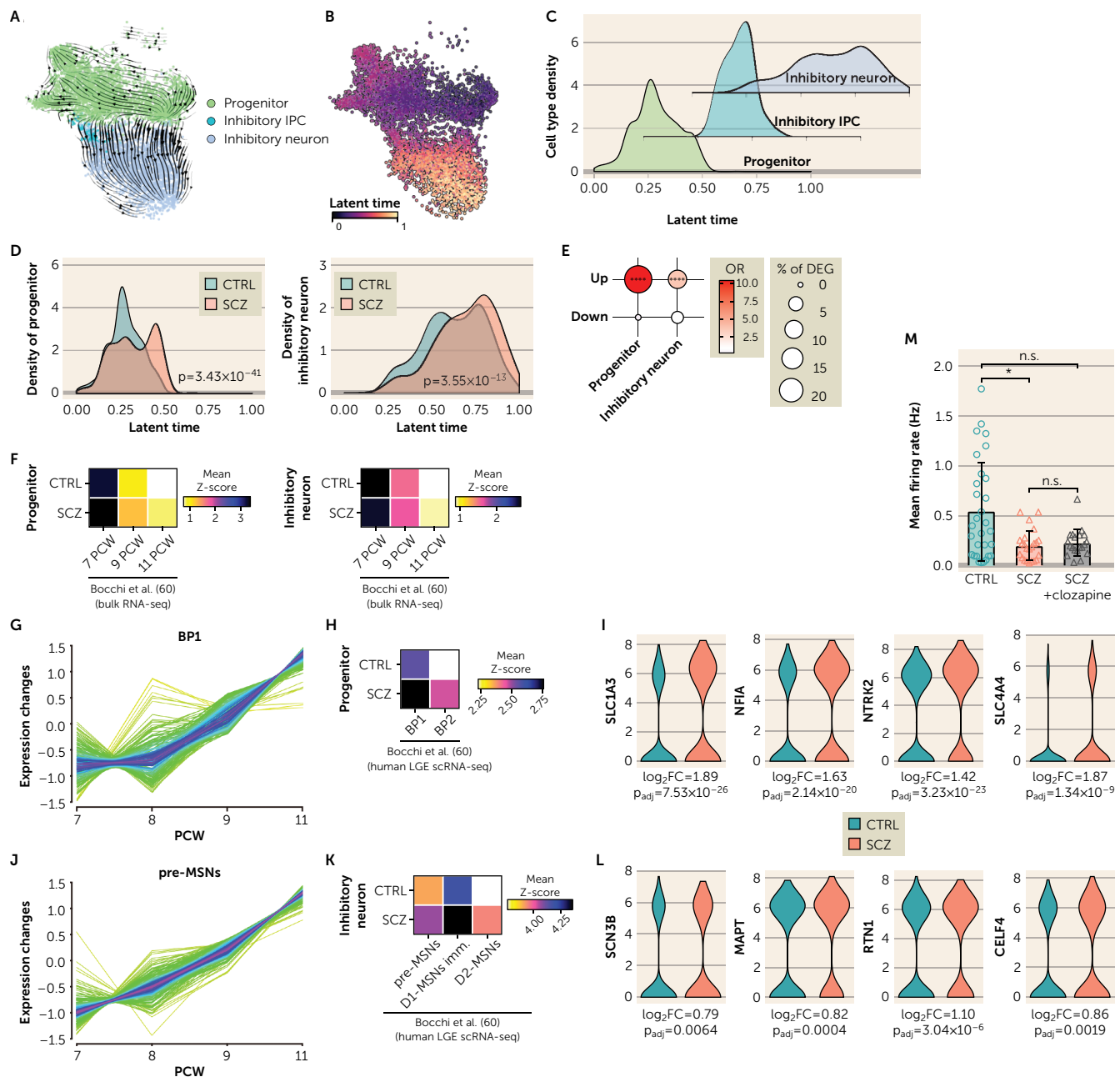
Concordant with these findings, schizophrenia VFOs exhibited a decrease in mean firing rate compared with control VFOs, indicating increased GABAergic inhibition in the neuronal network formed in schizophrenia VFOs (Figure 4M). Of note, clozapine, an atypical antipsychotic medication for schizophrenia, failed to rescue this phenotype (Figure 4M), potentially as a result of rare expression of dopamine receptors (see Figure S4H in the online supplement) because of the lack of nigral dopaminergic projections in VFOs.

VFOs Recapitulate the Brain Region–Specific Transcriptional Changes of Postmortem Brain Tissue From Individuals With Schizophrenia

The findings of perturbations of neurodevelopmental trajectory driven by schizophrenia-associated genes in schizophrenia VFOs (Figure 4D,E; see also and Figure S10E in the online supplement) and the identification of schizophrenia risk genes in DEGs in inhibitory neuronal cells between the control and schizophrenia groups (Figure 3F,H) led us to assess whether VFOs can reproduce the disease-associated changes in the postmortem tissue of the corresponding adult brain region, the caudate.

To address this challenge, we examined the overlap between cell type–specific DEGs in our VFO model with 1) schizophrenia GWAS-significant genes (3), 2) TWAS-significant genes from the postmortem caudate tissues (the BrainSeq consortium study [38], including donors of iPSC cohort) and DLPFC tissues (PsychENCODE study [56]), and 3) DEGs between control and schizophrenia samples from the postmortem caudate tissues (38) and DLPFC tissues (56) (see Table S13 in the online supplement). We did not identify significant enrichment of the cell

representative Gene Ontology (GO) terms enriched for upregulated and downregulated genes in SCZ progenitors compared with CTRL progenitors. The size of circles indicates a ratio of genes annotated in each GO term to all upregulated or downregulated genes in progenitors. Panel K is a dot plot showing representative GO terms enriched for upregulated and downregulated genes in SCZ inhibitory neurons compared with CTRL inhibitory neurons. The size of circles indicates a ratio of genes annotated in each GO term to all upregulated or downregulated genes in inhibitory neurons. Expression levels are shown in $\log_2$(CPM) (counts per million) in panels G and I. Dashed line indicates FDR=0.05 in panels J and K.

FIGURE 4. Accelerated differentiation of striatal inhibitory neuronal cells in schizophrenia ventral forebrain organoids[a]

[a] Panel A shows velocity estimates projected onto a UMAP (uniform manifold approximation and projection) of inhibitory neuronal cells (progenitor, inhibitory intermediate progenitor cell [IPC], and inhibitory neuron) in ventral forebrain organoids (VFOs) from four control (CTRL) lines and three schizophrenia (SCZ) lines. Panel B shows latent time projected onto a UMAP of inhibitory neuronal cells (progenitor, inhibitory IPC, and inhibitory neuron) in VFOs from four CTRL and three SCZ lines. Panel C shows the density of inhibitory neuronal cells applied across latent time estimated in panel B. Panel D shows the difference in the density of progenitors and inhibitory neurons between four CTRL and three SCZ lines across latent time (Kolmogorov-Smirnov test). Panel E is a dot plot showing the overlap between differentially expressed genes (DEGs) and 100 putative drivers in progenitors and inhibitory neurons. ****p=3.96×10^{-6} for progenitor; ****p=1.53×10^{-7} for inhibitory neuron; Fisher's exact test. OR=odds ratio. The size of circles indicates the percentage of DEGs overlapped with putative driver genes. Panel F shows matrix plots comparing expression of genes upregulated in human lateral ganglionic eminence (LGE) at postconception weeks (PCW) 7, 9, and 11 compared with medial ganglionic eminence and neocortex (60) in progenitors and inhibitory neurons in VFOs between four CTRL and three SCZ lines. Panel G shows a representative expression pattern of a cluster of genes (based on fuzzy c-means clustering) showing upregulation in basal progenitor 1 (BP1) in single-cell RNA sequencing (scRNA-seq) of human LGE (PCW 7–11) (60) during brain development. Panel H is a matrix plot comparing expression of genes that exhibited continuous upregulation in BP1 and BP2 in scRNA-seq of human LGE (PCW 7–11) (60) during brain development in VFO progenitors between CTRL and SCZ lines. Panel I shows representative expression of putative driver genes for progenitor upregulated in SCZ progenitors compared with CTRL progenitors that exhibited continuous upregulation in BP1 and/or BP2 in scRNA-seq of human LGE (PCW 7–11) (60) during brain development. Panel J shows a representative expression pattern of a cluster of genes (based on fuzzy c-means clustering) showing upregulation in pre–medium spiny neurons (pre-MSNs) in scRNA-seq of human LGE (PCW 7–11) (60) during brain development. Panel K is a matrix plot comparing expression of genes that exhibited continuous upregulation in pre-MSNs, immature D1 MSNs, and D2 MSNs in scRNA-seq of human LGE (PCW 7–11) (60) during brain

type–specific DEGs of VFOs within the set of GWAS-significant genes (see Table S13 in the online supplement). However, there was significant overlap of upregulated genes between inhibitory neurons of schizophrenia VFOs and postmortem caudate tissue of individuals with schizophrenia (odds ratio=3.38, p=0.0024) (Figure 5). Downregulated genes in inhibitory neurons of schizophrenia VFOs showed significant depletion for upregulated genes in postmortem caudate tissue of the schizophrenia patients (odds ratio=0.22, p=0.0215), and upregulated genes in progenitors of schizophrenia VFOs did not significantly overlap with these genes (Figure 5).

Upregulated genes in progenitors of schizophrenia VFOs exhibited marked overlap with upregulated genes in DLPFC of individuals with schizophrenia. In contrast, DEGs in inhibitory neurons of schizophrenia VFOs did not show enrichment for the DEGs in postmortem DLPFC (Figure 5), suggesting that 1) inhibitory neurons in VFOs develop the transcriptional signature of the caudate, the corresponding adult brain region of the donors, and 2) neurons have the ability to recapitulate, more so than do progenitors, brain region–specific disease-associated transcriptional changes in this VFO model.

Taken together, our findings raise the possibility that striatal neurons in individuals with schizophrenia carry abnormalities that originated during early brain development, and indicate that the VFO model can recapitulate these neurodevelopmental pathophysiological changes in a dish.
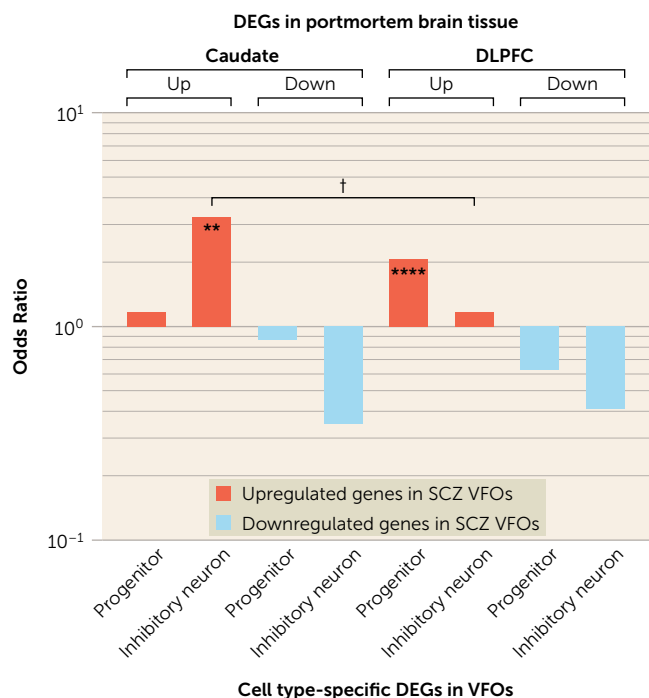
DISCUSSION

Genetic background is known as a large source of the variability between iPSC lines (78–80), which may obscure, exaggerate, or mislead the disease-related phenotypes observed in disease-modeling studies. Given the polygenic nature of schizophrenia and the significant overlap of PRSs between patients and healthy individuals in the general population (81), scaling back the influence of genetic variation is required for the iPSC-based modeling of schizophrenia, especially in cases lacking highly penetrant mutations. Analysis of twins discordant for the disorder (47, 82–84) and modeling the disorder with a relatively large-scale iPSC cohort are promising strategies (85). However, these strategies may not be easily applicable in the majority of studies because of the rarity of twin cases and the extremely large number of individuals theoretically required (79). Therefore, in the present study, we took an alternative strategy to maximize the difference in genetic risk between patients and control individuals. From among the postmortem brain and dural fibroblast donors in the LIBD brain repository, we selected four individuals with schizophrenia diagnoses and relatively high schizophrenia PRSs and four neurotypical individuals with low schizophrenia PRSs, and we analyzed iPSC-derived VFOs derived from this case-control cohort. While the number of iPSC lines analyzed in this study is at the lower end of current standards (86–88), our strategy of genetic PRS-based selection of cases and controls improved our power to identify genetic risk, if not disease-associated molecular and cellular alterations, with this iPSC-based model.

In addition to genomic heterogeneity, it has also been a challenging endeavor to demonstrate the validity and disease relevancy of the iPSC-based model for adult-onset psychiatric disorders, considering the maximum maturity of neural cells that can be differentiated from human iPSCs (34). Our strategy enabled us to analyze iPSC-derived brain organoids and postmortem brain tissue from the same individuals, and thus to evaluate whether the organoid model can recapitulate any disease-relevant gene expression changes identified in the postmortem adult brain tissue. In addition to these advantages, there are challenges in dural fibroblast–derived iPSCs, which may be problematic. One is that dural fibroblasts grow more slowly than dermal fibroblasts and may decrease the reprogramming efficiency. Another is that postmortem interval seems to be negatively correlated with the growth of fibroblasts, which potentially affects the reprogramming efficiency with episomal vectors, but not with SeV.

With a defined case-control dura-derived iPSC cohort, we have demonstrated that at the transcription level, inhibitory neurons in VFOs are mature enough to recapitulate certain disease-associated changes seen in adults. We identified significant overlap of genes upregulated in schizophrenia between inhibitory neurons of VFOs and postmortem caudate tissue of individuals diagnosed with schizophrenia, but not with postmortem DLPFC (Figure 5). This finding shows the ability of VFOs to recapitulate brain region–specific pathophysiological changes observed in adult patient brains, despite the discrepancy in cellular maturity between the brain organoids and postmortem brains, and despite the fact that postmortem brains reflect the consequences of a lifelong illness and pharmacological treatment. Although further studies are required to address these difficulties—including 1) cell type–specific gene expression profiles in the iPSC-derived brain organoids with donor-matched postmortem caudate tissues with a larger cohort, and 2) examining gene co-expression patterns and dynamics in VFOs and postmortem

development in VFO inhibitory neurons between CTRL and SCZ lines. Panel L shows representative expression of putative driver genes of inhibitory neurons upregulated in SCZ inhibitory neurons compared with CTRL inhibitory neurons, which exhibited continuous upregulation in pre-MSNs, immature D1 MSNs, and/or D2 MSNs in scRNA-seq of human LGE (PCW 7–11) (60) during brain development. Panel M shows mean firing rate of VFOs from four CTRL and four SCZ lines, measured on multi-electrode array at days 75–82 for the untreated condition and at days 96–103 for clozapine treatment (N=1–5 VFOs per line per recording, N=30 for CTRL; N=23 for untreated SCZ; N=20 for SCZ with clozapine treatment). SCZ VFOs were treated with 1 μM clozapine for 2 weeks. *p=0.0358; n.s.=not significant; Kruskal-Wallis test with post hoc Dunn's multiple comparisons test.

FIGURE 5. Inhibitory neurons in ventral forebrain organoids from individuals with schizophrenia recapitulate transcriptional perturbations in the schizophrenia postmortem caudate[a]

[a] The plot shows enrichment and depletion of differentially expressed genes (DEGs) in progenitors and inhibitory neurons in schizophrenia (SCZ) ventral forebrain organoids (VFOs) compared with control (CTRL) VFOs with DEGs in postmortem caudate tissue (38) and dorsolateral prefrontal cortex (DLPFC) tissue (56) in schizophrenia patients compared with neurotypical control individuals. **p=0.00243; ****p=1.65×10^{-5}; Fisher's exact test. †p=0.01183, hypergeometric test.

brain tissues—the present study implicates aberrant fetal striatogenesis in adult-onset schizophrenia pathogenesis.

Neuronal progenitors and inhibitory neurons in VFOs showed transcriptional similarity to human ganglionic eminences and the developing striatum (Figure 1I–L), suggesting that these cells are at an early stage of human striatal development. Regardless of the immature identity of the cells, putative driver genes for progenitors and inhibitory neurons, which regulate transcriptional switches upon differentiation or maturation, showed remarkable overlap with schizophrenia risk–associated genes (see Figure S10E in the online supplement). Cell type–specific profiling of gene expression in VFOs revealed that the alterations in the developmental trajectory of inhibitory neurons begins at the progenitor stage (Figures 3 and 4). Given that several studies have demonstrated the importance of schizophrenia-associated genes in human brain development (28, 29), our findings support other evidence that schizophrenia risk starts accumulating in utero and is coded by genomic sequences involved in striatal pathogenesis, and that patient brains maintain certain consequences of in utero neurodevelopmental perturbations throughout life.

In this study, we generated VFOs from iPSCs to simulate human striatal development in a dish. With a case-control iPSC cohort of four individuals with schizophrenia and four neurotypical control individuals with nonoverlapping PRSs, in which the patients had high schizophrenia PRSs and the control individuals low PRSs, we identified alterations in the striatal neurodevelopmental trajectory as a molecular underpinning of the striatal pathogenesis of schizophrenia. To our knowledge, this is the first study that has evaluated the validity of the iPSC-based brain organoid model of schizophrenia with corresponding postmortem brain tissue from the same donors. Given the limited number of case and control individuals analyzed in our iPSC cohort, however, this study may not be able to adequately reduce the undesired effects of genomic variation between individuals. For instance, there were several cell types that arose from specific iPSC lines, such as dorsal organizers and inhibitory IPCs on day 150 (see Figure S8 in the online supplement). Additionally, the differential expression analysis in VFOs in this study was performed with a single batch of samples. Further replication of our findings with a large iPSC cohort would help confirm the disease relevancy of our findings. Moreover, striatal neurons in our organoid model were at an immature stage. The consequences of altered striatal development in the pathogenesis of schizophrenia at mature stages remain to be elucidated.

Although organoids can simulate human brain development more appropriately than two-dimensional neuronal cultures, it is still a simplified model compared to in vivo brain development. Simulating developmental trajectory combined with genetic perturbations, and integrating multidimensional organoid and brain tissue data sets, would have a great impact on predicting the consequences of neurodevelopmental perturbations that are encoded by genomic risk in the patient brains. Further studies using our strategy of analyzing the brain organoids and corresponding postmortem brain tissue from the same individuals with a larger case-control cohort, in combination with the tracing of human brain development in silico, could advance our understanding of the neurodevelopmental origin of schizophrenia and accelerate the search for novel therapeutic targets of the disorder.

AUTHOR AND ARTICLE INFORMATION

Lieber Institute for Brain Development, Baltimore (Sawada, Barbosa, Araujo, McCord, D'Ignazio, Benjamin, Sheehan, Feltrin, Arora, Brandtjen, Kleinman, Hyde, Weinberger, Paquola, Erwin); Department of Neurology (D'Ignazio, Benjamin, Kleinman, Hyde, Weinberger, Paquola, Erwin), Department of Psychiatry and Behavioral Sciences (Benjamin, Kleinman, Hyde, Weinberger), and Department of Neuroscience (Weinberger, Erwin), Johns Hopkins School of Medicine, Baltimore; South Australian Health and Medical Research Institute, Laboratory for Human Neurophysiology and Genetics, Adelaide (Zabolocki, Bardy); Flinders Health and Medical Research Institute, College of Medicine and Public Health, Flinders University, Adelaide (Zabolocki, Bardy).

Send correspondence to Dr. Sawada (tomoyo.sawada@libd.org) and Dr. Erwin (jennifer.erwin@libd.org).

REFERENCES

1. Jablensky A, Kirkbride JB, Jones PB: Schizophrenia: the epidemiological horizon; in Schizophrenia, 3rd ed. Edited by Weinberger DR, Harrison PJ. Hoboken, NJ, Wiley-Blackwell, 2011, pp 185–225

2. Kahn RS, Sommer IE, Murray RM, et al: Schizophrenia. Nat Rev Dis Primers 2015; 1:15067

3. Trubetskoy V, Pardiñas AF, Qi T, et al: Mapping genomic loci implicates genes and synaptic biology in schizophrenia. Nature 2022; 604:502–508

4. Birnbaum R, Weinberger DR: Genetic insights into the neurodevelopmental origins of schizophrenia. Nat Rev Neurosci 2017; 18:727–740

5. Millan MJ, Andrieux A, Bartzokis G, et al: Altering the course of schizophrenia: progress and perspectives. Nat Rev Drug Discov 2016; 15:485–515

6. Räsänen N, Tiihonen J, Koskuvi M, et al: The iPSC perspective on schizophrenia. Trends Neurosci 2022; 45:8–26

7. Woodward ND, Rogers B, Heckers S: Functional resting-state networks are differentially affected in schizophrenia. Schizophr Res 2011; 130:86–93

8. Skudlarski P, Jagannathan K, Anderson K, et al: Brain connectivity is not only lower but different in schizophrenia: a combined anatomical and functional approach. Biol Psychiatry 2010; 68:61–69

9. Fornito A, Zalesky A, Pantelis C, et al: Schizophrenia, neuroimaging, and connectomics. Neuroimage 2012; 62:2296–2314

10. Stevens JR: Neuropathology of schizophrenia. Arch Gen Psychiatry 1982; 39:1131–1139

11. Harrison PJ: The neuropathology of schizophrenia: a critical review of the data and their interpretation. Brain 1999; 122:593–624

12. Weinberger DR, Berman KF, Suddath R, et al: Evidence of dysfunction of a prefrontal-limbic network in schizophrenia: a magnetic resonance imaging and regional cerebral blood flow study of discordant monozygotic twins. Am J Psychiatry 1992; 149:890–897

13. Simpson EH, Kellendonk C, Kandel E: A possible role for the striatum in the pathogenesis of the cognitive symptoms of schizophrenia. Neuron 2010; 65:585–596

14. McCutcheon RA, Abi-Dargham A, Howes OD: Schizophrenia, dopamine, and the striatum: from biology to symptoms. Trends Neurosci 2019; 42:205–220

15. Groenewegen HJ: The basal ganglia and motor control. Neural Plast 2003; 10:107–120

16. Seeman P, Lee T, Chau-Wong M, et al: Antipsychotic drug doses and neuroleptic/dopamine receptors. Nature 1976; 261:717–719

17. Gerfen CR: The neostriatal mosaic: multiple levels of compartmental organization. Trends Neurosci 1992; 15:133–139

18. Tepper JM, Bolam JP: Functional diversity and specificity of neostriatal interneurons. Curr Opin Neurobiol 2004; 14:685–692

19. Graveland GA, DiFiglia M: The frequency and distribution of medium-sized neurons with indented nuclei in the primate and rodent neostriatum. Brain Res 1985; 327:307–311

20. Wu Y, Parent A: Striatal interneurons expressing calretinin, parvalbumin, or NADPH-diaphorase: a comparative study in the rat, monkey, and human. Brain Res 2000; 863:182–191

21. Kawaguchi Y, Wilson CJ, Augood SJ, et al: Striatal interneurones: chemical, physiological, and morphological characterization. Trends Neurosci 1995; 18:527–535

22. Deacon TW, Pakzaban P, Isacson O: The lateral ganglionic eminence is the origin of cells committed to striatal phenotypes: neural transplantation and developmental evidence. Brain Res 1994; 668:211–219

23. Olsson M, Campbell K, Wictorin K, et al: Projection neurons in fetal striatal transplants are predominantly derived from the lateral ganglionic eminence. Neuroscience 1995; 69:1169–1182

24. Olsson M, Björklund A, Campbell K: Early specification of striatal projection neurons and interneuronal subtypes in the lateral and medial ganglionic eminence. Neuroscience 1998; 84:867–876

25. Anderson SA, Qiu M, Bulfone A, et al: Mutations of the homeobox genes Dlx-1 and Dlx-2 disrupt the striatal subventricular zone and differentiation of late born striatal neurons. Neuron 1997; 19:27–37

26. Marin O, Anderson SA, Rubenstein JL: Origin and molecular specification of striatal interneurons. J Neurosci 2000; 20:6063–6076

27. Xu Q, Cobos I, De La Cruz E, et al: Origins of cortical interneuron subtypes. J Neurosci 2004; 24:2612–2622

28. Birnbaum R, Jaffe AE, Hyde TM, et al: Prenatal expression patterns of genes associated with neuropsychiatric disorders. Am J Psychiatry 2014; 171:758–767

29. Jaffe AE, Shin J, Collado-Torres L, et al: Developmental regulation of human cortex transcription and its clinical relevance at single base resolution. Nat Neurosci 2015; 18:154–161

30. Autism Spectrum Disorders Working Group of the Psychiatric Genomics Consortium: Meta-analysis of GWAS of over 16,000 individuals with autism spectrum disorder highlights a novel locus at 10q24.32 and a significant overlap with schizophrenia. Mol Autism 2017; 8:21

31. de Jong JO, Llapashtica C, Genestine M, et al: Cortical overgrowth in a preclinical forebrain organoid model of CNTNAP2-associated autism spectrum disorder. Nat Commun 2021; 12:4087

32. Urresti J, Zhang P, Moran-Losada P, et al: Cortical organoids model early brain development disrupted by 16p11.2 copy number variants in autism. Mol Psychiatry 2021; 26:7560–7580

33. Zhang W, Ma L, Yang M, et al: Cerebral organoid and mouse models reveal a RAB39b-PI3K-mTOR pathway-dependent dysregulation of cortical development leading to macrocephaly/autism phenotypes. Genes Dev 2020; 34:580–597

34. Gordon A, Yoon SJ, Tran SS, et al: Long-term maturation of human cortical organoids matches key early postnatal transitions. Nat Neurosci 2021; 24:331–342

35. Choi SW, Mak TSH, O'Reilly PF: Tutorial: a guide to performing polygenic risk score analyses. Nat Protoc 2020; 15:2759–2772

36. Sawada T, Benjamin KJM, Brandtjen AC, et al: Generation of four postmortem dura-derived iPS cell lines from four control individuals with genotypic and brain-region-specific transcriptomic data available through the BrainSEQ consortium. Stem Cel Res 2020; 46:101806

37. Collado-Torres L, Burke EE, Peterson A, et al: Regional heterogeneity in gene expression, regulation, and coherence in the frontal cortex and hippocampus across development and schizophrenia. Neuron 2019; 103:203–216.e8

38. Benjamin KJM, Chen Q, Jaffe AE, et al: Analysis of the caudate nucleus transcriptome in individuals with schizophrenia highlights effects of antipsychotics and new risk genes. Nat Neurosci 2022; 25: 1559–1568

39. Jaffe AE, Gao Y, Deep-Soboslay A, et al: Mapping DNA methylation across development, genotype, and schizophrenia in the human frontal cortex. Nat Neurosci 2016; 19:40–47

40. Bliss LA, Sams MR, Deep-Soboslay A, et al: Use of postmortem human dura mater and scalp for deriving human fibroblast cultures. PLoS One 2012; 7:e45282

41. Wray NR, Goddard ME, Visscher PM: Prediction of individual genetic risk to disease from genome-wide association studies. Genome Res 2007; 17:1520–1528

42. Schizophrenia Working Group of the Psychiatric Genomics Consortium: Biological insights from 108 schizophrenia-associated genetic loci. Nature 2014; 511:421–427

43. International Schizophrenia Consortium, Purcell SM, Wray NR, et al: Common polygenic variation contributes to risk of schizophrenia and bipolar disorder. Nature 2009; 460:748–752

44. Ursini G, Punzi G, Chen Q, et al: Convergence of placenta biology and genetic risk for schizophrenia. Nat Med 2018; 24:792–801

45. Okita K, Matsumura Y, Sato Y, et al: A more efficient method to generate integration-free human iPS cells. Nat Methods 2011; 8: 409–412

46. Ito N, Hendriks WT, Dhakal J, et al: Decreased N-TAF1 expression in X-linked dystonia-parkinsonism patient-specific neural stem cells. Dis Model Mech 2016; 9:451–462

47. Sawada T, Chater TE, Sasagawa Y, et al: Developmental excitation-inhibition imbalance underlying psychoses revealed by single-cell analyses of discordant twins-derived cerebral organoids. Mol Psychiatry 2020; 25:2695–2711

48. Lancaster MA, Knoblich JA: Generation of cerebral organoids from human pluripotent stem cells. Nat Protoc 2014; 9:2329–2340

49. Trujillo CA, Gao R, Negraes PD, et al: Complex oscillatory waves emerging from cortical organoids model early human brain network development. Cell Stem Cell 2019; 25:558–569

50. Arlotta P, Quadrato G, Sherwood JL: Long-term culture and electrophysiological characterization of human brain organoids. Protocol Exchange, 2017. https://doi.org/10.1038/protex.2017.049

51. Stoeckius M, Zheng S, Houck-Loomis B, et al: Cell hashing with barcoded antibodies enables multiplexing and doublet detection for single cell genomics. Genome Biol 2018; 19:224

52. Srivastava A, Malik L, Smith T, et al: Alevin efficiently estimates accurate gene abundances from dscRNA-seq data. Genome Biol 2019; 20:65

53. Wolf FA, Angerer P, Theis FJ: SCANPY: large-scale single-cell gene expression data analysis. Genome Biol 2018; 19:15

54. Traag VA, Waltman L, van Eck NJ: From Louvain to Leiden: guaranteeing well-connected communities. Sci Rep 2019; 9: 5233

55. Raudvere U, Kolberg L, Kuzmin I, et al: g:Profiler: a web server for functional enrichment analysis and conversions of gene lists (2019 update). Nucleic Acids Res 2019; 47:W191–W198

56. Gandal MJ, Zhang P, Hadjimichael E, et al: Transcriptome-wide isoform-level dysregulation in ASD, schizophrenia, and bipolar disorder. Science 2018; 362:eaat8127

57. La Manno G, Soldatov R, Zeisel A, et al: RNA velocity of single cells. Nature 2018; 560:494–498

58. Bergen V, Lange M, Peidli S, et al: Generalizing RNA velocity to transient cell states through dynamical modeling. Nat Biotechnol 2020; 38:1408–1414

59. Kumar L, E Futschik M: Mfuzz: a software package for soft clustering of microarray data. Bioinformation 2007; 2:5–7

60. Bocchi VD, Conforti P, Vezzoli E, et al: The coding and long noncoding single-cell atlas of the developing human fetal striatum. Science 2021; 372:eabf5759

61. BrainSeq: A Human Brain Genomics Consortium: BrainSeq: neurogenomics to drive novel target discovery for neuropsychiatric disorders. Neuron 2015; 88:1078–1083

62. Bhaduri A, Andrews MG, Mancia Leon W, et al: Cell stress in cortical organoids impairs molecular subtype specification. Nature 2020; 578:142–148

63. Kanton S, Boyle MJ, He Z, et al: Organoid single-cell genomic atlas uncovers human-specific features of brain development. Nature 2019; 574:418–422

64. Miura Y, Li MY, Birey F, et al: Generation of human striatal organoids and cortico-striatal assembloids from human pluripotent stem cells. Nat Biotechnol 2020; 38:1421–1430

65. Yu Y, Zeng Z, Xie D, et al: Interneuron origin and molecular diversity in the human fetal brain. Nat Neurosci 2021; 24:1745–1756

66. Fleck JS, Sanchís-Calleja F, He Z, et al: Resolving organoid brain region identities by mapping single-cell genomic data to reference atlases. Cell Stem Cell 2021; 28:1148–1159.e8

67. Graybiel AM, Ragsdale CW: Histochemically distinct compartments in the striatum of human, monkeys, and cat demonstrated by acetylthiocholinesterase staining. Proc Natl Acad Sci USA 1978; 75: 5723–5726

68. Crittenden JR, Graybiel AM: Basal ganglia disorders associated with imbalances in the striatal striosome and matrix compartments. Front Neuroanat 2011; 5:59

69. Blaesse P, Airaksinen MS, Rivera C, et al: Cation-chloride cotransporters and neuronal function. Neuron 2009; 61:820–838

70. Cuomo ASE, Seaton DD, McCarthy DJ, et al: Single-cell RNA-sequencing of differentiating iPS cells reveals dynamic genetic effects on gene expression. Nat Commun 2020; 11:810

71. Rouhani F, Kumasaka N, de Brito MC, et al: Genetic background drives transcriptional variation in human induced pluripotent stem cells. PLoS Genet 2014; 10:e1004432

72. Notaras M, Lodhi A, Fang H, et al: The proteomic architecture of schizophrenia iPSC-derived cerebral organoids reveals alterations in GWAS and neuronal development factors. Transl Psychiatry 2021; 11:541

73. Chen C, Meng Q, Xia Y, et al: The transcription factor POU3F2 regulates a gene coexpression network in brain tissue from patients with psychiatric disorders. Sci Transl Med 2018; 10: eaat8178

74. Pearl JR, Colantuoni C, Bergey DE, et al: Genome-scale transcriptional regulatory network models of psychiatric and neurodegenerative disorders. Cell Syst 2019; 8:122–135.e7

75. Mistry M, Gillis J, Pavlidis P: Genome-wide expression profiling of schizophrenia using a large combined cohort. Mol Psychiatry 2013; 18:215–225

76. Blair JD, Hockemeyer D, Doudna JA, et al: Widespread translational remodeling during human neuronal differentiation. Cell Rep 2017; 21:2005–2016

77. Chau KF, Shannon ML, Fame RM, et al: Downregulation of ribosome biogenesis during early forebrain development. eLife 2018; 7: e36998

78. Carcamo-Orive I, Hoffman GE, Cundiff P, et al: Analysis of transcriptional variability in a large human iPSC library reveals genetic and non-genetic determinants of heterogeneity. Cell Stem Cell 2017; 20:518–532

79. Kilpinen H, Goncalves A, Leha A, et al: Common genetic variation drives molecular heterogeneity in human iPSCs. Nature 2017; 546: 370–375

80. Schwartzentruber J, Foskolou S, Kilpinen H, et al: Molecular and functional variation in iPSC-derived sensory neurons. Nat Genet 2018; 50:54–61

81. Sullivan PF, Geschwind DH: Defining the genetic, genomic, cellular, and diagnostic architectures of psychiatric disorders. Cell 2019; 177: 162–183

82. Nakazawa T, Kikuchi M, Ishikawa M, et al: Differential gene expression profiles in neurons generated from lymphoblastoid B-cell

line-derived iPS cells from monozygotic twin cases with treatment-resistant schizophrenia and discordant responses to clozapine. Schizophr Res 2017; 181:75–82

83. Toritsuka M, Yoshino H, Makinodan M, et al: Developmental dysregulation of excitatory-to-inhibitory GABA-polarity switch may underlie schizophrenia pathology: a monozygotic-twin discordant case analysis in human iPS cell-derived neurons. Neurochem Int 2021; 150:105179

84. Koskuvi M, Lehtonen Š, Trontti K, et al: Contribution of astrocytes to familial risk and clinical manifestation of schizophrenia. Glia 2022; 70:650–660

85. Readhead B, Hartley BJ, Eastwood BJ, et al: Expression-based drug screening of neural progenitor cells from individuals with schizophrenia. Nat Commun 2018; 9:4412

86. Kathuria A, Lopez-Lengowski K, McPhie D, et al: Disease-specific differences in gene expression, mitochondrial function, and mitochondria-endoplasmic reticulum interactions in iPSC-derived cerebral organoids and cortical neurons in schizophrenia and bipolar disorder. Discov Ment Health 2023; 3:8

87. Notaras M, Lodhi A, Dündar F, et al: Schizophrenia is defined by cell-specific neuropathology and multiple neurodevelopmental mechanisms in patient-derived cerebral organoids. Mol Psychiatry 2022; 27:1416–1434

88. Page SC, Sripathy SR, Farinelli F, et al: Electrophysiological measures from human iPSC-derived neurons are associated with schizophrenia clinical status and predict individual cognitive performance. Proc Natl Acad Sci U S A 2022; 119:e2109395119